RESULTS AND DISCUSSION

4.1 Optimization of medium components using statistical design tools

The medium components for rapamycin production were analyzed by a statistical software Minitab version 15.1.0.0. Central composite Design (CCD) tool of Minitab was used for development of experimental designs which were performed and then they were compared with the predicted values. The experiments designed by CCD were used as data set for Artificial Neural Network and Genetic Algorithm (ANN-GA) based optimization of the values.

4.1.1 CCD based experimental design

Central composite design was used for design of experiments based on regression analysis. The levels of medium components were major nutrient source and precursor was optimized. The effects of three independent variables on rapamycin production were analyzed. The analysis was carried out at five different levels which were -α, -1, 0, +1 and +α as shown in Table 4.1. The value of $\alpha = 2^{n/4}$, where n signifies the number of variables used for CCD study. Total 20 experiments were designed using a full factorial central composite design, containing 8 cube points (2^3), 6 centre points (4 in cube and 2 in axial positions) and 6 star points (3x2 = 6) as shown in Table 4.2. The relationship between the independent variable and response (rapamycin production) was calculated using a polynomial equation. The quadratic regression model can be represented by the eq. 4.1.1 as follows:

$$Y = \rho_0 + \sum_{i=1}^{n} \rho_i X_i + \sum_{i=1}^{n} \rho_{ii} X_i^2 + \sum_{i=1}^{n} \sum_{j=1}^{n} \rho_{ij} X_i X_j \quad \text{- (4.1.1)}$$

Where, ρ_0 denotes model constant, n is number of variables, ρ_i is linear effect of input terms X_i, ρ_{ii} is quadratic effect of input variables X_i while ρ_{ij} is effect of linear interactions between input terms X_i and X_j.

Table 4.1: Five levels of media components concentrations used for CCD

Factors codes	Factors	Pre-lower level (-α) (g/L)	Lower level (-1) (g/L)	Mid-level (0) (g/L)	Higher level (+1) (g/L)	Post-higher level (+α) (g/L)
X1	Mannose	14.95	17	20	23	25.04
X2	Soyabean Meal	11.59	15	20	25	28.41
X3	L-lysine	1.59	5	10	15	18.40

Experiments were conducted according to the design proposed by CCD in 250 mL shake flasks containing 50 mL production medium. The design and the experimental results have been summarized in Table 4.2. By applying the multiple regression analysis on the experimental data, a second order polynomial equation was obtained as shown by eq. (4.1.2).

Table 4.2: Central Composite Design in coded units to study interactive effects of the significant parameters

Run	Mannose concentration (X_1)	Soyabean Meal concentration (X_2)	L-lysine concentration (X_3)	Experimental Rapamycin concentration (mg/L)
1	0	0	+α	230 ± 4.4
2	0	0	0	268 ± 3.5
3	-1	1	1	206 ± 5.2
4	0	0	0	271 ± 5.2

5	0	+α	0	230 ± 4.9
6	-1	-1	-1	187 ± 5.2
7	-1	-1	1	215 ± 4.5
8	0	0	0	265 ± 6.7
9	0	0	0	267 ± 6.4
10	1	-1	-1	208 ± 5.7
11	-1	1	-1	218 ± 5.4
12	+α	0	0	247 ± 6.7
13	1	1	-1	224 ± 4.8
14	1	-1	1	248 ± 5.9
15	0	0	0	269 ± 6.3
16	0	0	0	271 ± 5.3
17	1	1	1	235 ± 4.4
18	-α	0	0	209 ± 3.9
19	0	0	-α	198 ± 5.1
20	0	-α	0	212 ± 4.3

The following equation explains the effect of medium components and their interactions on the production of rapamycin from *S. hygroscopicus* NRRL 5491:

$$Y = -250.33 + 31.213\ X_1 + 11.786\ X_2 + 9.619\ X_3 - 4.431\ X_1^2 - 1.765\ X_2^2 - 10.206\ X_3^2 - 10.235\ X_1X_2 + 7.315\ X_1X_3 - 1.522\ X_2X_3 \quad -(4.1.2)$$

Where, X_1 is mannose, X_2 is soyabean meal, X_3 is L-lysine and Y is concentration of rapamycin produced (response activity).

4.1.1.1 Regression analysis of the interactions between the media components

Regression analysis was carried out to evaluate the predicted interactions between the medium components using Minitab software. The result obtained by analysis has been shown in Table 4.3.

Table 4.3: Model coefficient estimated by multiple linear regressions

Model Term	Parameter estimate	Standard error coefficient	t-value	p-value
Intercept	250.330	2.287	109.446	0.000
Mannose	31.213	1.518	20.568	0.000
Soyabean Meal	11.786	1.518	7.767	0.000
Lysine	9.619	1.518	6.339	0.000
Mannose*Mannose	-4.431	1.477	-3.000	0.013
Soyabean Meal*Soyabean Meal	-1.765	1.477	-1.195	0.260
Lysine*Lysine	-10.206	1.477	-6.909	0.000
Mannose*Soyabean Meal	-10.235	1.983	-5.162	0.000
Mannose*Lysine	7.315	1.983	3.689	0.004
Soyabean Meal*Lysine	-1.522	1.983	-0.768	0.460

Coefficients having larger magnitude of the t value and a smaller p value can be associated with more significance. Also, p value less than 0.05 exhibits the significance of coefficient at 5% confidence level. The results were analyzed using the ANOVA as appropriate to the experimental design used. The statistical analysis shows that the interaction of mannose with soyabean meal ($p = 0$) and mannose with L-lysine ($p = 0.004$) were found to be very significant.

The appropriateness of the model was checked by coefficient of determination, R^2, which implies that the sample variation of 98.41% for rapamycin production is attributed to the medium components and also only 1.59% of the total variation is not explained by the model. This explains the significance of the model optimization process.

4.1.2 Use of Artificial Intelligence tool for optimization

The design proposed by CCD and the result obtained experimentally was used as input data to carry out optimization using Artificial Neural Network-Genetic algorithm (ANN-GA) hybrid methodology.

4.1.2.1 Development of ANN based model for rapamycin production

Artificial Neural Network based modeling relies on the non-linear interactions of bioprocess variables [Franco-Lara *et al.*, 2006]. ANN has been used as feed forward iteration method for variables whose interactions with other parameters have not been mathematically described. In this study, 20 data sets designed by CCD were used as input variables. Out of these 12 were used as training set, 4 as validation set while the remaining 4 were used as independent test sets. The multi layer perceptron (MLP) network has three input nodes (L = 3) for representing the three process variables (mannose concentration, soyabean meal concentration, L-lysine concentration) and one output node (N = 1) representing the rapamycin concentration (mg/L) at the end of a batch. The process data for MLP-based modeling was generated by carrying out a number of fermentation runs by varying the input conditions. ANN model provided accurate predictions by minimizing the learning error which was done by increasing the number of epochs.

The data were trained in 1077 epoch with R value of 0.9998 (shown in Fig.4.1.) and mean square error value of 0.305, shown in Fig.4.2. The results depicts that ANN based training shows better correlation with the experimental rapamycin level compared to that using only RSM regression model.

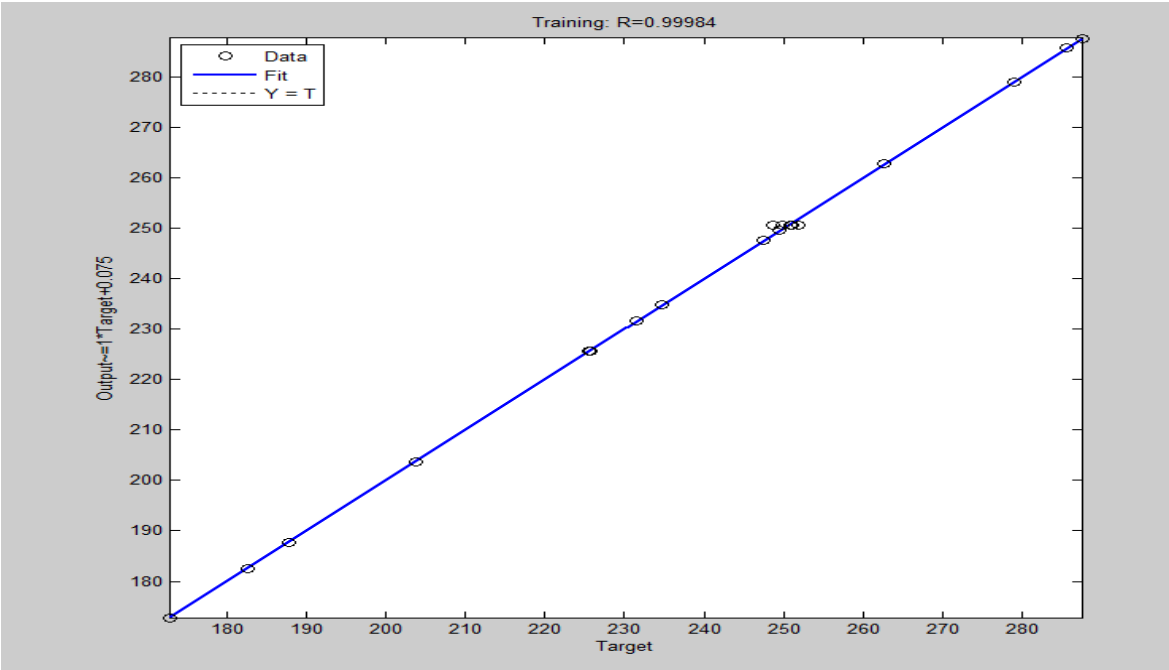

Fig.4.1. Result of training of data set with 619 epoch using ANN

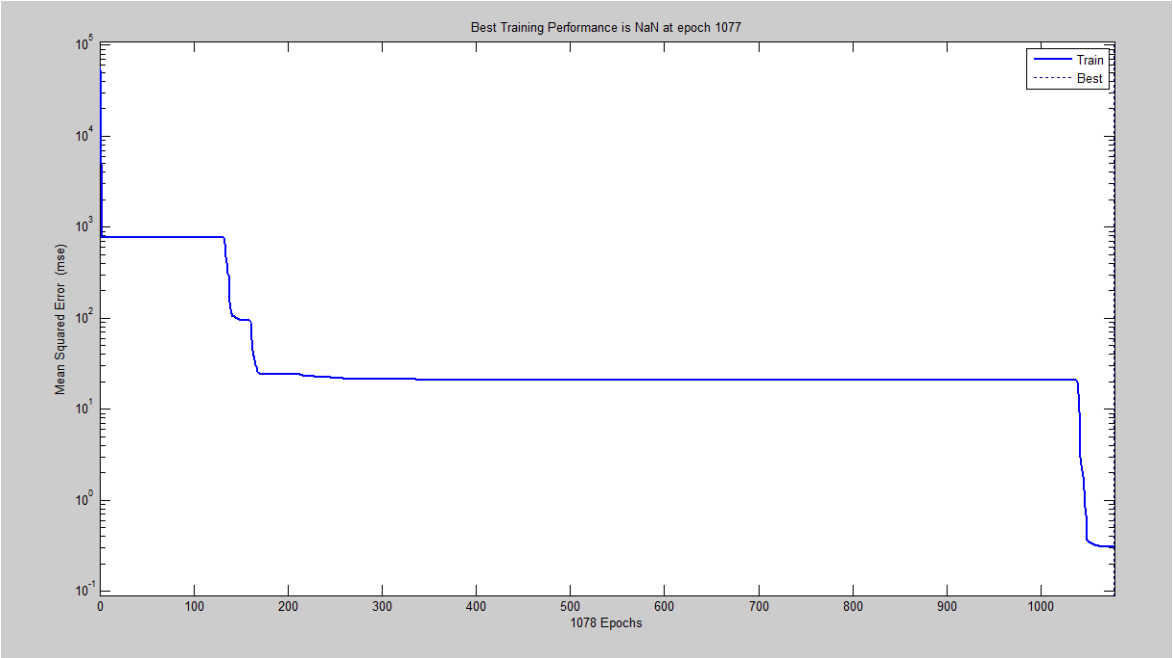

Fig.4.2. Graph showing training epoch cycles vs. calculated mean square error of the supervised training for the designed ANN

4.1.2.2 Optimization by genetic algorithm using ANN model

In this study, genetic algorithm tool in MATLAB (Version 7.0, Mathworks., Inc. MA, USA) was employed. The trained data's (by ANN) fitness was evaluated by fitness evaluation function. The parameters which were taken for the GA optimization had population size of 10, mutation rate of 0.1 and uniform cross overrate of 0.8.

In order to validate the optimization results five experiments were performed under the predicted optimal condition. Results of GA based optimization and their experimental outcomes are shown in Table 4.4. One sample student t-test was carried out for all 5 runs. Results show that the difference between the hypothetical mean (predicted value) and the observed mean (experimental value) was not statistically significant, as the p-value was greater than 0.05. Thus, the optimal concentrations for the medium components were obtained by Run 1.

Fig. 4.3 shows that multiple iterations of GA led to convergence of the best optimal solution to the mean optimal solution. This value is the global optimal solution for the optimization problem. Thus, the optimal concentrations for the three components obtained from the model are 25.47, 15.39 and 17.48 g/L for mannose, soyabean meal and L-lysine concentration respectively. The optimization using ANN model linked with GA is found to be the more effective for rapamycin production with a high degree of accuracy.

Thus, the medium composition for rapamycin production was optimized using ANN-GA based hybrid optimization technique and this optimized medium was used for all further studies.

Table 4.4: Comparison of predicted and experimentally obtained GA result for concentration of rapamycin produced

	Mannose concentr-ation (g/L)	Soyabean Meal concentration (g/L)	L-Lysine concentr-ation (g/L)	Predicted concentration (mg/L)	Experimental concentration (mg/L)	p-value
Run 1	25.4707	15.3964	17.4837	323	320	0.323
Run 2	25.3961	13.1726	16.7709	339	317	0.006
Run 3	25.3403	12.1420	16.1184	346	319	0.0005
Run 4	25.3616	13.5815	15.7472	335	315	0.0005
Run 5	25.0659	12.3552	16.3694	338	317	0.0119

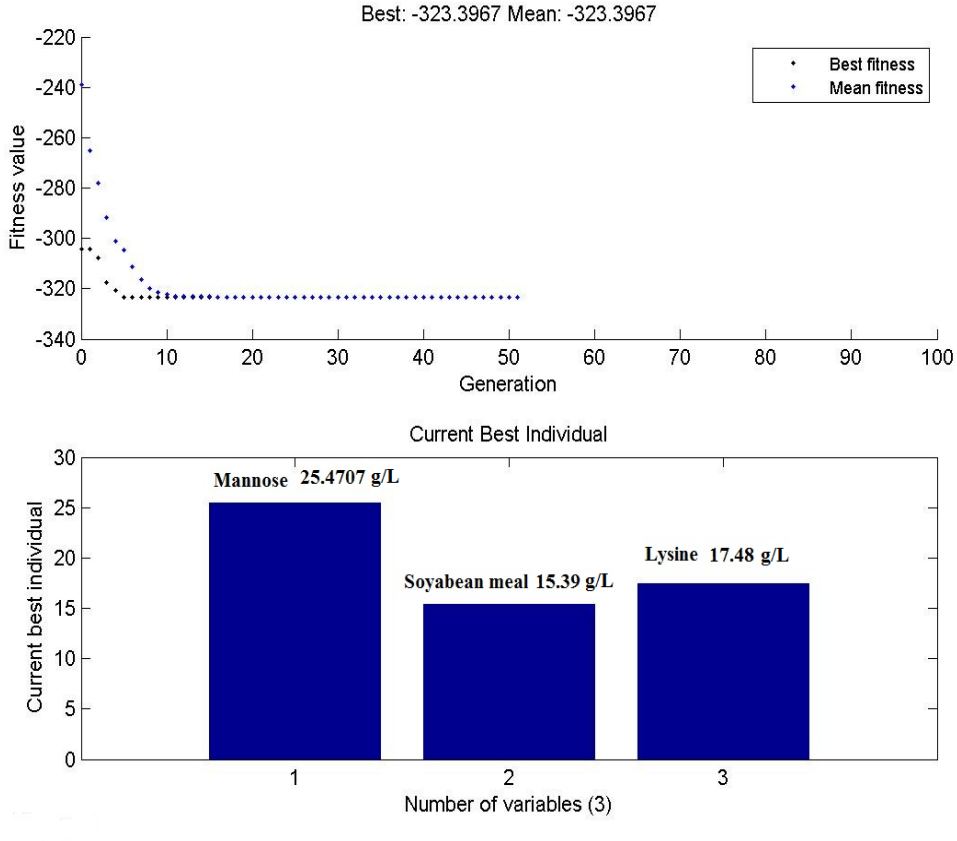

Fig.4.3. Fitness plot showing the GA iterations based on fitness function to achieve the optimum solution over several generations. GA predicted result for optimized concentration of mannose, soyabean meal and L-lysine for the best individual

4.2 Rapamycin production in 3 L bioreactor

Rapamycin production was carried out in batch mode using 3 L stirred tank reactor (STR) (Scigenics India, India) with working volume capacity of 2 L (Fig. 3.4). The fermentation in STR was carried out using final optimized media described in the previous study. pH was maintained at 6.0, working temperature was maintained at 28°C, stirring speed of 400 rpm and aeration rate was maintained at 1.0 vvm. The pH was automatically controlled at 6.0 by using 0.1 M HCl and 0.1 M NaOH. 0.5% Silicone oil was used as antifoam agent.

Mathematical modeling tool was used to determine the variation in growth and production profile by varying the reducing sugar concentration. The experiments were carried out using varying concentrations of carbon source (mannose) which range from 15 g/L to 30 g/L to study its effect on fermentation kinetics in a 3L bioreactor.

4.2.1 Modeling of cell growth, rapamycin production and substrate utilization

Curve fitting was done using non-linear curve fitting function in Origin 8.0 Software. In this study, an unstructured kinetic model was used to correlate the rapamycin production with reducing sugar concentration. The unstructured kinetic model has been most extensively used for microbial system due to their simplicity and wider applicability.

Fig 4.4 Production of rapamycin in 3L Stirred tank reactor (Scigenics, India)

The growth profile of *S. hygroscopicus* was analyzed using logistic equation. Logistic equation was applied which was based on following assumptions:

i) Mannose is the only limiting substrate for the complete fermentation process ii) L-lysine acts a precursor for rapamycin production and it does not affect the mannose uptake by *S.hygroscopicus* iii) Cellular growth and biosynthesis of metabolites are dependent on availability of mannose as substrate. Based on these assumptions, the logistic equation can be written as:

$$\frac{dx}{dt} = \mu_{max}\left(1 - \frac{x}{x_{max}}\right)x \qquad \text{- (4.2.1)}$$

Where, x represents biomass concentration at time t, x_{max} is maximum cell growth in terms of dry cell mass concentration which can be attained and μ_{max} is maximum specific cell growth rate. On integrating eq (4.2.1), and assuming $x = x_o$ at t =0 we get [Elibol *et al.*, 1999],

$$x = \frac{x_o e^{\mu max\ t}}{\left\{1-\left(\frac{x_o}{x_{max}}\right)(1-e^{\mu max\ t})\right\}} \qquad \text{- (4.2.2)}$$

Eq. 4.2.2 is logistic model and applies for both exponential as well as stationary phase. This model was used to fit the dry cell mass concentration data as shown in Fig 4.5 (A-D). The fitted model showed the three phases of growth which are lag, log and stationary phase.

On the other hand production of rapamycin was evaluated using Luedeking –Piret model which correlates the product concentration to biomass concentration. It partitions the production rate between growth and non-growth phase of batch culture. Luedeking- Piret

model [Luedeking *et al.*, 1959] was proposed for lactic acid formation by *Lactobacillus delbrueckii* as follows:

$$\frac{dP}{dt} = \alpha \frac{dx}{dt} + \beta x \qquad \text{-(4.2.3)}$$

In eq. (4.2.3), α is coefficient of growth associated product formation rate whereas β is coefficient of non- growth associated product formation rate. Thus, this equation details the relation of product formation with growth, based on the value of β which can be positive negative or zero which indicates that product is non-growth associated, completely growth associated or degrades during stationary phase respectively. On integration eq. (4.2.3) can be written as [Elibol *et al.*, 1999]:

$$P - P_o = \alpha(x - x_o) + \beta \frac{x_{max}}{\mu_{max}} ln \left(\frac{x_{max} - x_o}{x_{max} - x}\right) \qquad \text{-(4.2.4)}$$

Putting the value of x from eq. (4.2.2) and $P_o = 0$, we get [Elibol *et al.*, 1999]

$$P = \alpha x_o \left[\frac{e^{\mu_m t}}{1-\left(x_o/x_m\right)(1-e^{\mu_m t})} - 1\right] + \beta \frac{x_m}{\mu_m} \ln \left[1 - \frac{x_o}{x_m}(1 - e^{\mu_m t})\right] \qquad \text{-(4.2.5)}$$

Thus, eq. (4.2.5) was used for modeling of rapamycin concentration during batch production in a bioreactor as shown in Fig 4.5 (A-D). Result showed that the model predicted that production should increase with time upto 120 hours but the experimental findings showed that the product concentration did not rise significantly after 96 hours. Similar results were obtained by other workers also during modeling of antibiotic production [Elibol *et al.*, 1999, Lu *et al.*, 2011]. This can be due to carbon catabolite repression as reported in other studies [Sanchez *et al.*, 2010].

In order to model substrate utilization kinetics the relation proposed by Pirt was used [Pirt, 1965]. According to this model, growth of microorganism depends on the carbon source which gets incorporated into the biomass, channels biosynthesis of metabolites and facilitates basal maintenance requirements. Substrate utilization kinetics was determined using the following function:

$$-\frac{ds}{dt} = \frac{1}{Y_{x/s}}\frac{dx}{dt} + m_s x \qquad \text{- (4.2.6)}$$

Where $Y_{(x/s)}$ = dx/ds (g biomass/g substrate) , m_s = specific maintenance coefficient (h^{-1}).

Eq. (4.2.6) can be expressed in the following form on integration [Elibol *et al.*, 1999]:

$$S_t = S_o - \frac{x - x_o}{Y_{x/s}} - m_s \frac{x_m}{\mu_m} \ln\left(\frac{x_m - x_o}{x_m - x}\right) \qquad \text{- (4.2.7)}$$

Putting the value of x from eq. (4.2.2) in Eq. (4.2.7) following equation can be obtained [Elibol *et al.*, 1999]

$$S_t = S_o - \gamma C(t) - \delta D(t) \qquad \text{- (4.2.8)}$$

In eq. (4.2.8),

$$C(t) = x_o \left[\frac{e^{\mu_m t}}{1 - \left(x_o/x_m\right)(1 - e^{\mu_m t})} - 1\right]$$

$$\text{and } D(t) = \frac{x_m}{\mu_m} ln\left[1 - \frac{x_o}{x_m}(1 - e^{\mu_m t})\right] \qquad \text{-(4.2.9)}$$

In eq. (4.2.8), δ = m_s, which was determined by the equation $\delta = \frac{-(ds/dt)_{st.}}{x_m}$, and $\gamma = 1/Y_{x/s}$.

Eq. 4.2.8 was used to fit the substrate consumption data for rapamycin production as shown in Fig 4.5 (A-D). The values of m_s were calculated as 0.0031, 0.0058, 0.0064, 0.0069 g-man/g-cells/h for initial concentration of mannose as 15, 20, 25 and 30 g/L respectively.

Fig. 4.5 (A-D) shows the three states of growth of microorganism: lag phase, log phase and stationary phase which was obtained when dry cell mass data was fitted into logistic model. The experiments were carried out for 120 hours. Lag phase is characterized by period where no growth of microorganism is observed. This is followed by logarithmic phase or exponential phase where the cells grow with maximum specific growth rate for most of the period. Rapamycin production initiated only after 24 hours of growth of *S.hygroscopicus* but continued in the stationary phase. The stationary phase is marked by no apparent growth of microorganism.

From the model fitted graphs, it can be observed that initial mannose concentration affected the cell growth as well as rapamycin production. The correlation coefficient (R^2) values were obtained for each fitting of kinetic models as shown in Table 4.5. The values of R^2 show that the growth, production and substrate consumption data were well fitted in their respective models.

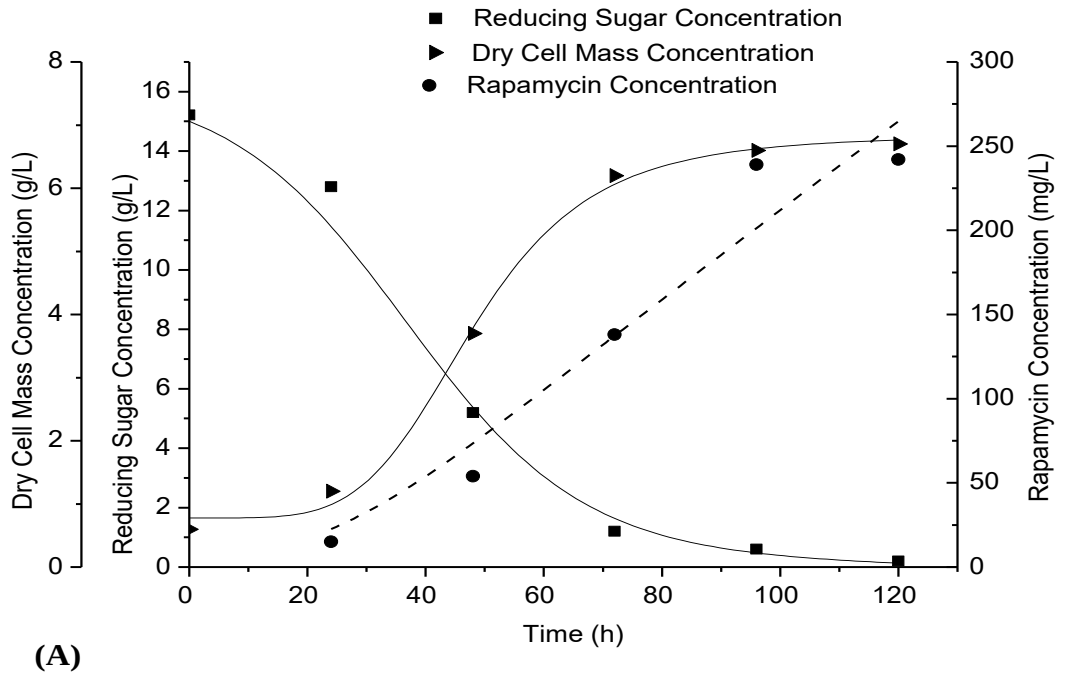

Fig. 4.5 (A): Model fitting of experimental observations of dry cell mass, reducing sugar concentration and rapamycin production during batch production at initial mannose concentration 15 g/L

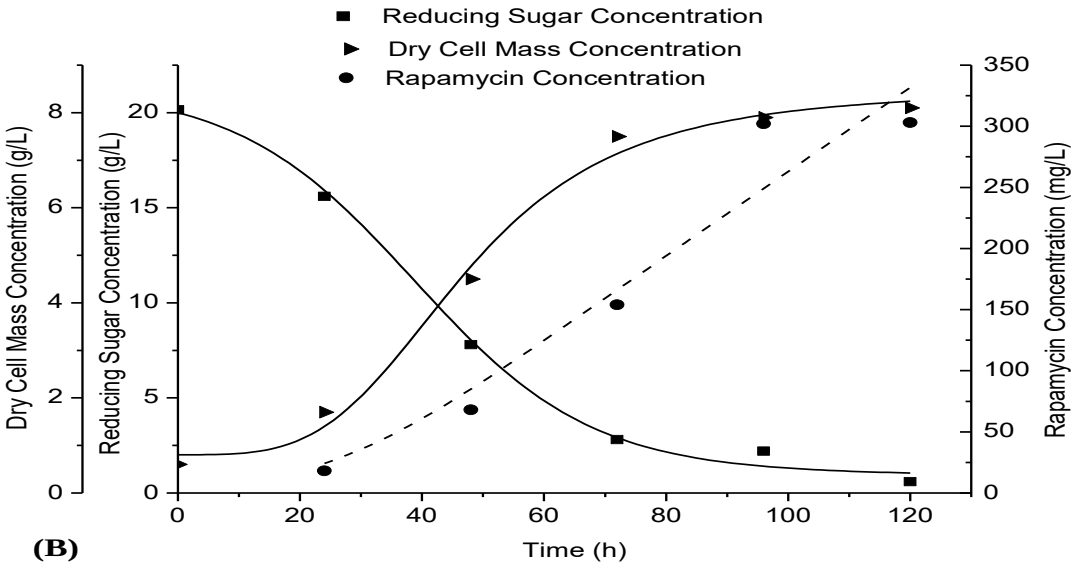

Fig. 4.5 (B): Model fitting of experimental observations of dry cell mass, reducing sugar concentration and rapamycin production during batch production at initial mannose concentration 20 g/L

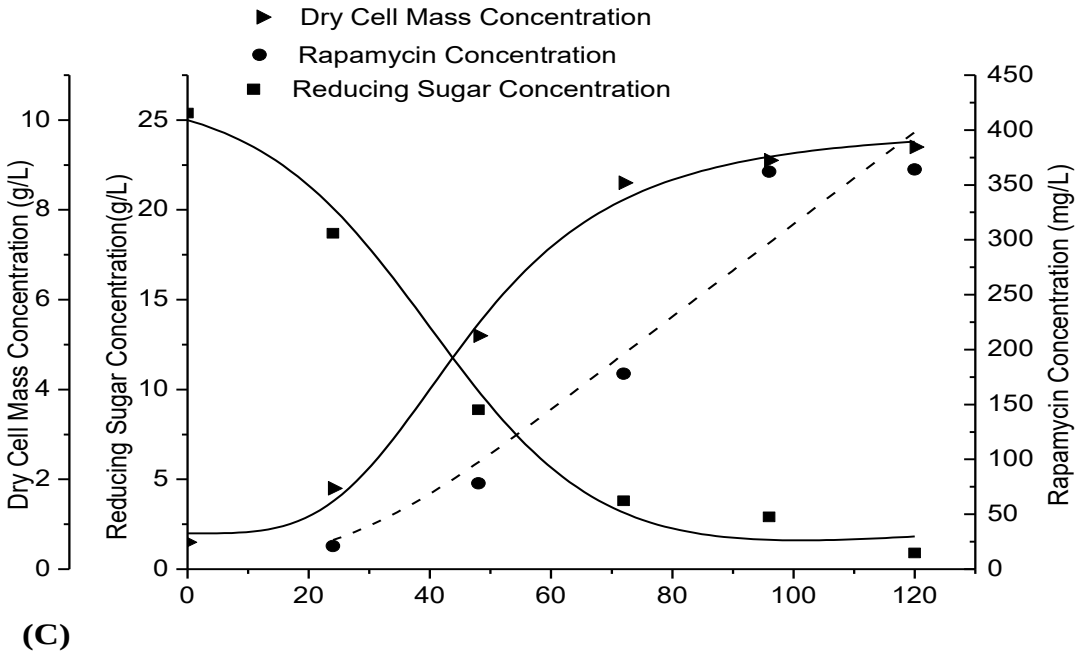

(C)

Fig 4.5 (C): Model fitting of experimental observations of dry cell mass, reducing sugar concentration and rapamycin production during batch production at initial mannose concentration 25 g/L

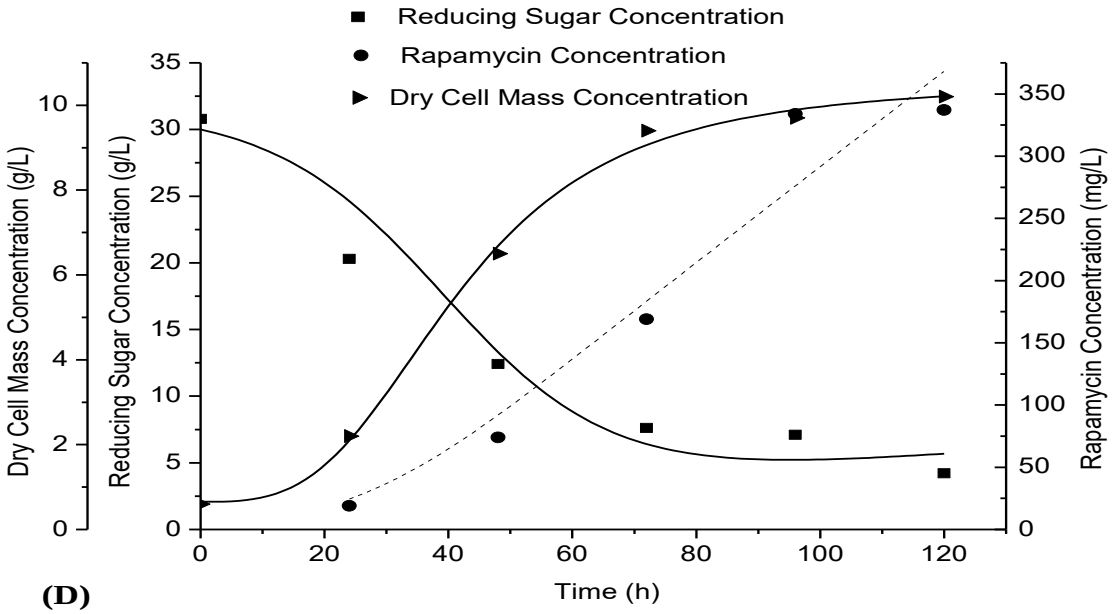

(D)

Fig 4.5 (D): Model fitting of experimental observations of dry cell mass, reducing sugar concentration and rapamycin production during batch production at initial mannose concentration 30 g/L

Table 4.5 Determination of goodness of fit using R^2 values for growth, production and substrate consumption

Parameters	Models	Initial mannose concentration (So)	R^2
Dry Cell Mass Concentration (X)	$x = \frac{x_o e^{\mu_{max}\ t}}{\left\{1 - \left(\frac{x_o}{x_{max}}\right)(1 - e^{\mu_{max}\ t})\right\}}$	15	0.97
		20	0.96
		25	0.98
		30	0.97
Substrate Concentration (S_t)	$S_t = S_o - \gamma C(t) - \delta D(t)$	15	0.97
		20	0.98
		25	0.98
		30	0.93
Product Concentration (P)	$P = \alpha x_o \left[\frac{e^{\mu_m t}}{1-\left(x_o/x_m\right)(1-e^{\mu_m t})} - 1\right] + \beta \frac{x_m}{\mu_m} \ln\left[1 - \frac{x_o}{x_m}(1 - e^{\mu_m t})\right]$	15	0.93
		20	0.92
		25	0.92
		30	0.94

4.2.2 Evaluation of the kinetic parameters

Different kinetic parameters associated with growth, rapamycin production and mannose utilization were evaluated.

4.2.2.1 Evaluation of growth kinetics parameter

On rearranging equation eq. (4.2.2), we get eq. (4.2.10) as follows [Elibol *et al.*, 1999]:

$$ln\frac{x}{(x_{max} - x)} = \mu_{max}\, t - ln\left(\frac{x_{max}}{x_0} - 1\right) \qquad \text{- (4.2.10)}$$

Using Eq. (4.2.10) a plot between $ln\frac{x}{(x_{max} - x)}$ and t was drawn which gave a linear graph with slope = μ_{max} and intercept as $ln\left(\frac{x_{max}}{x_0} - 1\right)$ as shown in Fig 4.6.

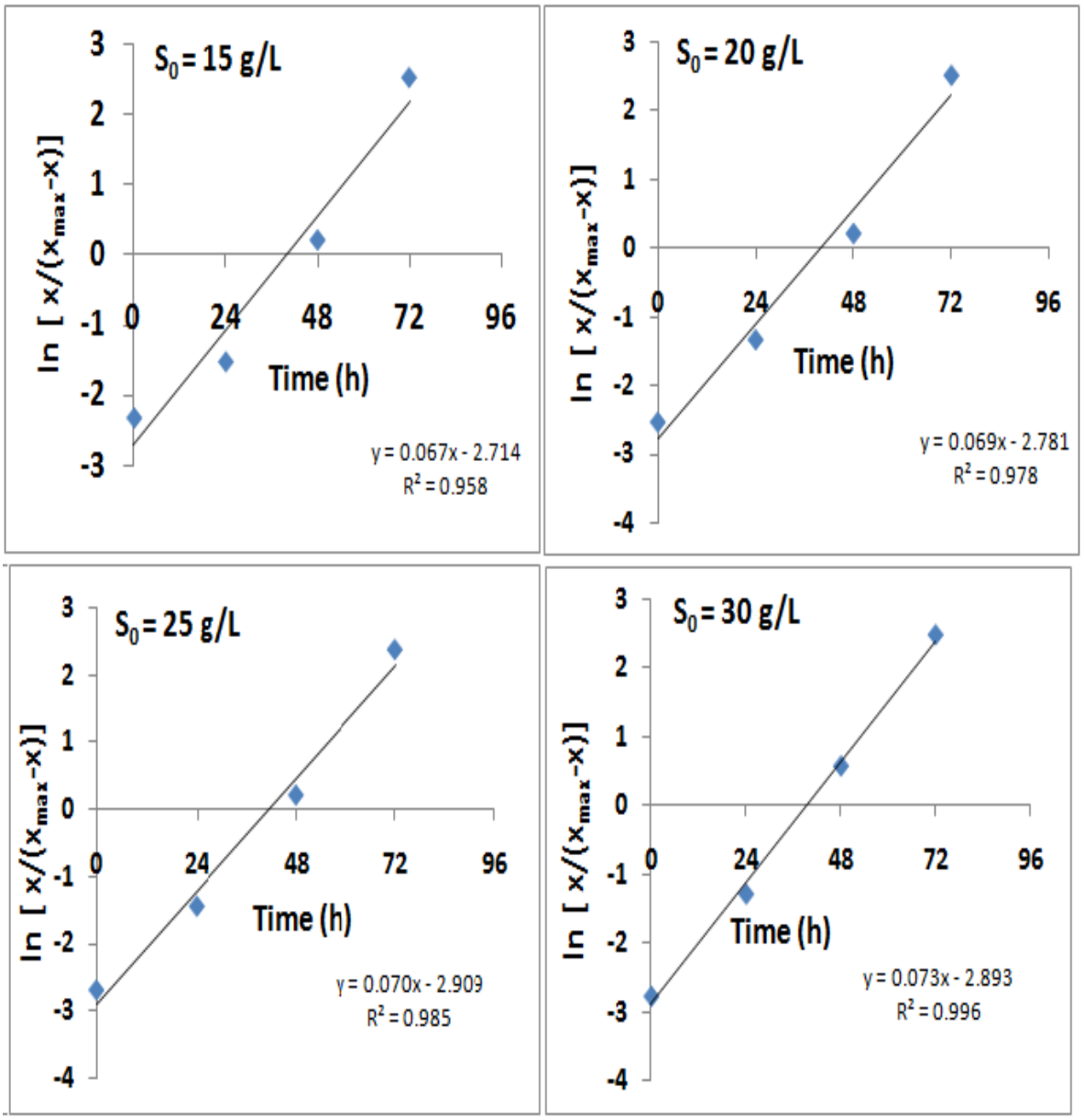

Fig 4.6 Plot for determination of maximum specific growth rate (μ_{max}) at different initial mannose concentration (So = 15-30 g/L)

The values of μ_{max} and x_o were calculated for different initial mannose concentration and have been summarized in Table 4.6.

Table 4.6 Determination of μ_{max} and x_o at different initial mannose concentration

Initial mannose concentration (S_o) (g/L)	Maximum specific growth rate (μ_{max}) (h^{-1})	Initial cell mass concentration (x_o) (g/L)
15	$0.067 \pm 1 \times 10^{-3}$	0.54± 0.005
20	$0.069 \pm 7 \times 10^{-4}$	0.53±0.004
25	$0.07 \pm 8 \times 10^{-4}$	0.52±0.008
30	$0.073 \pm 1 \times 10^{-4}$	0.55±0.006

Thus, from Table 4.6 it can be inferred that maximum specific growth rate increased from 0.067 to 0.073 as the mannose concentration increased from 15 g/L to 30 g/L. The value of calculated initial cell mass concentration (x_o) was found to be lower than experimental value which was about 0.6 g/L for each case. This lowering can be associated to the fact that calculated value is the measure of the viable cells [Pazouki *et al.*, 2008].

4.2.2.2 Evaluation of product formation kinetics

Kinetic parameters related to rapamycin production were determined to investigate the effect of different initial mannose concentration in stirred tank bioreactor.

Eq. (4.2.5) can be represented as [Elibol *et al.*, 1999]

$$P = \alpha A(t) + \beta B(t) \qquad \text{-(4.2.11)}$$

Where A(t) = $x_o \left[\frac{e^{\mu_m t}}{1-\left({}^{x_o}/_{x_m}\right)(1-e^{\mu_m t})} - 1\right]$ and B(t) = $\frac{x_m}{\mu_m} \ln\left[1 - \frac{x_o}{x_m}(1 - e^{\mu_m t})\right]$

In eq. (4.2.11) the value of β was determined by the relation $\beta = \frac{({}^{dP}/_{dt})_{st.}}{x_m}$ whereas the value of α was calculated by finding the slope of the plot of [P-βB(t)] versus A(t). The result has been shown in Table 4.7.

Table 4.7 Determination of production related kinetics at different initial mannose concentration

Kinetic Parameters	Values			
	So =15 g/L	So =20 g/L	So =25 g/L	So =30 g/L
α (mg g-man^{-1})	3.82	3.96	3.91	2.72
β (mg g-man^{-1} h^{-1})	0.32	0.38	0.41	0.34
q_p (mg g-cells^{-1} h^{-1})	0.33	0.33	0.34	0.2

From the table 4.7, it may be inferred that rapamycin production is mixed fermentation type product as it is produced both during growth as well as stationary phase. Similar result has been obtained in case of other antibiotics also [Lu *et al.*, 2011]. Also, the value of α, β and q_p decreases as the initial substrate concentration increases from 25 g/L to 30 g/L. Thus, 25 g/L was found to be optimum initial mannose concentration for maximum production of rapamycin in 3L stirred tank bioreactor. The overall biomass yield was found to be 0.38 g-cells g-man^{-1} while the overall product yield was found to be 14.86 mg-rap g-man^{-1} when 25 g/L of mannose was used as initial substrate concentration.

Another relation between product formation and biomass concentration was evaluated by eq. (4.2.12) derived from eq. (4.2.4) as [Singh *et al.*, 2014]:

$$\gamma = \alpha x_{max} \left[(\theta - \theta_o) + \sigma \, ln \left(\frac{1-\theta_o}{1-\theta} \right) \right] \qquad \text{-(4.2.12)}$$

where, $\gamma = P$, $\theta = \frac{x}{x_{max}}$ and $\sigma = \frac{\beta}{\alpha \mu_{max}}$

Based on conditions, if σ is negative the graph of γ versus θ, will be convex having γ as the peak value which shows degradation of product during the stationary phase. The value of σ = 0 indicates that product formation is fully growth associated. When σ is positive, the graph will not follow the linear rising trend instead it will rise more rapidly with increase in value of θ and forms a concave plot. The values of σ varied from 0.01 to 1.56 when the initial substrate concentration was changed from 15 g/L to 30 g/L which showed that rapamycin production occurs during stationary phase. The variation of γ with θ for different initial mannose concentration has been shown in Fig 4.7 which followed a concave pattern [Singh *et al.*, 2014].

Fig 4.7 depicts that as the value of biomass concentration (x) approaches towards maximum biomass concentration (x_m), an increase in rapamycin concentration was found which shows that significant amount of rapamycin is produced during stationary phase.

The values kinetic parameters and regression coefficient of fitting (R^2) of eq. 4.2.12 into the rapamycin concentration data have been shown in Table 4.8 which showed that the model well fitted into the product concentration values.

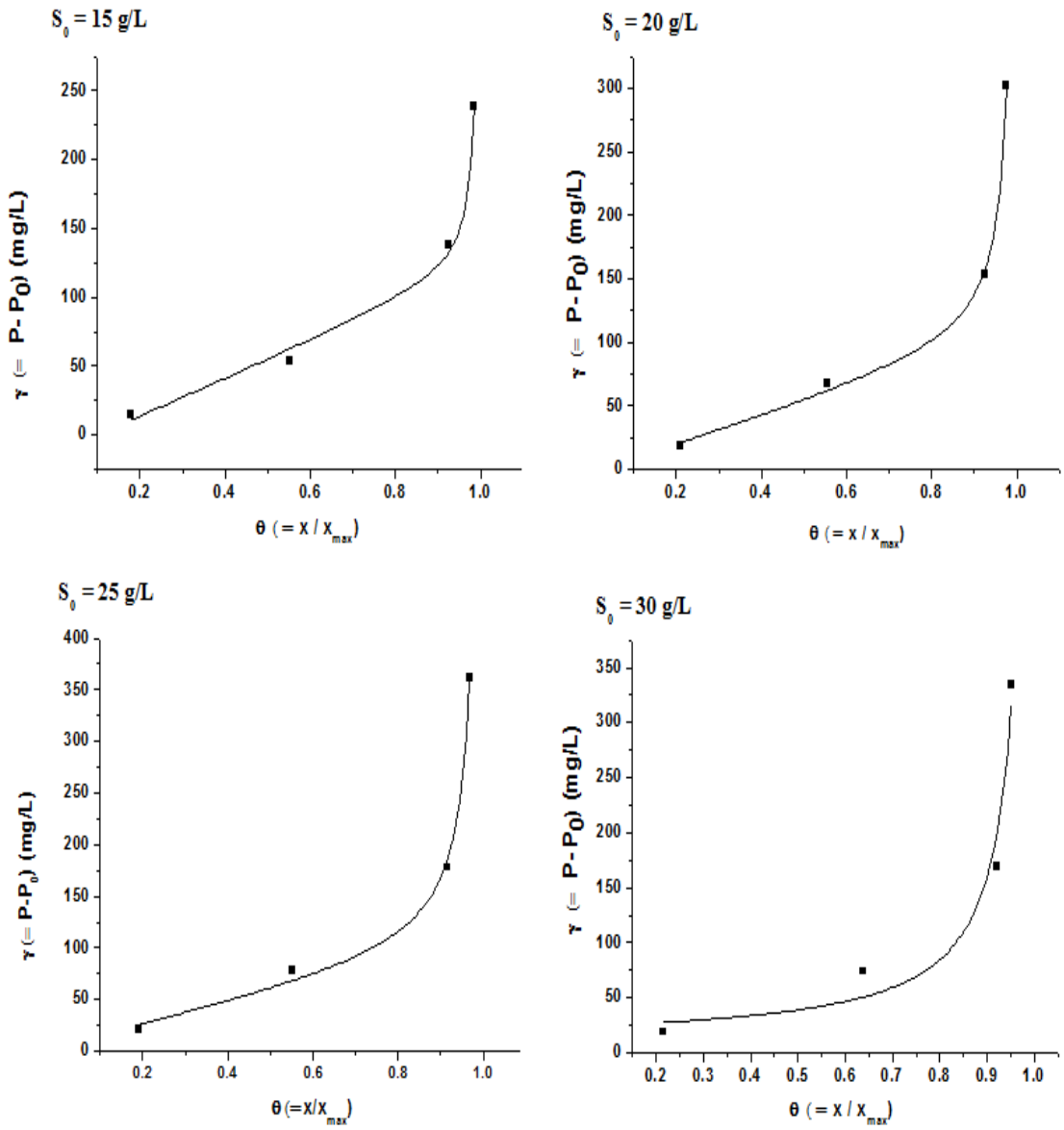

Fig 4.7 Graph between γ and θ at initial sugar concentrations 15 g/L, 20 g/L, 25 g/L and 30 g/L

Table 4.8 Evaluation of production of rapamycin during stationary phase

Parameters	Values			
	So =15 g/L	So =20 g/L	So =25 g/L	So =30 g/L
θ_0	0.08	0.065	0.055	0.053
σ	0.01	0.05	0.09	1.56
R^2	0.988	0.996	0.94	0.916

Thus, increase in mannose concentration from 15g/L to 25 g/L led to increase in rapamycin concentration from 242 mg/L to 364 mg/L but further increase in the reducing sugar concentration did not enhance the production. A further increase in reducing sugar concentration led to reduction in rapamycin production to 337 mg/L. The decrement in rapamycin concentration can be supported by the results of previous findings in other reports where polyketides and other secondary metabolites concentrations have been found to reduce with increase in sugar content [Sanchez *et al.*, 2010, Sujatha *et al.*, 2005]. Carbon catabolite repression has been previously reported in antibiotic synthesis [Ruiz *et al.*, 2010].

4.2.3 Dissolved oxygen profile during rapamycin production in 3L fermentor

Dissolved oxygen (DO) is an important parameter for production of secondary metabolites by *Streptomyces spp.* as they are aerobic microorganisms [Jarai *et al.*, 1969, Lechevalier *et al.*, 1970]. Fig 4.8 shows the variation of dissolved oxygen concentration with rapamycin production and was correlated to biomass concentration and reducing sugar concentration at initial mannose concentration 25 g/L.

It can be clearly observed from the Fig. 4.8, that as the culture reached growth phase, there was a sharp decline in dissolved oxygen curve which was caused by increased oxygen

demand in the culture. As the microorganism reached the stationary phase, the dissolved oxygen concentration again spiked and reached around 35% towards the end of trophophase at about 72 hours. During the stationary phase, the dissolved oxygen concentration increased but did not reach the initial concentration due to viscous nature of fermentation broth and other mass transfer limiting parameters of the broth.

The variation of volumetric oxygen transfer coefficient (k_La) with dissolved oxygen concentration was also determined. It can be observed that, k_La decreased upto 72 hours, after which the value of k_La is maintained almost at a constant level till the end of fermentation process.

It is evident (Fig 4.9) that though the DO level increased after the cells entered the stationary phase, k_La did not increase due to viscous nature of the broth attributed to the mycelial growth of *S. hygroscopicus*. Similar profile of k_La decline in *Streptomycete* fermentation have been reported in earlier studies [Tuffile *et al.*, 1970]. Earlier reports of decrease in volumetric oxygen transfer coefficient due to increase in apparent viscosity of the broth during Cephalosporin C production supported the above results [Mishra *et al.*, 2005].

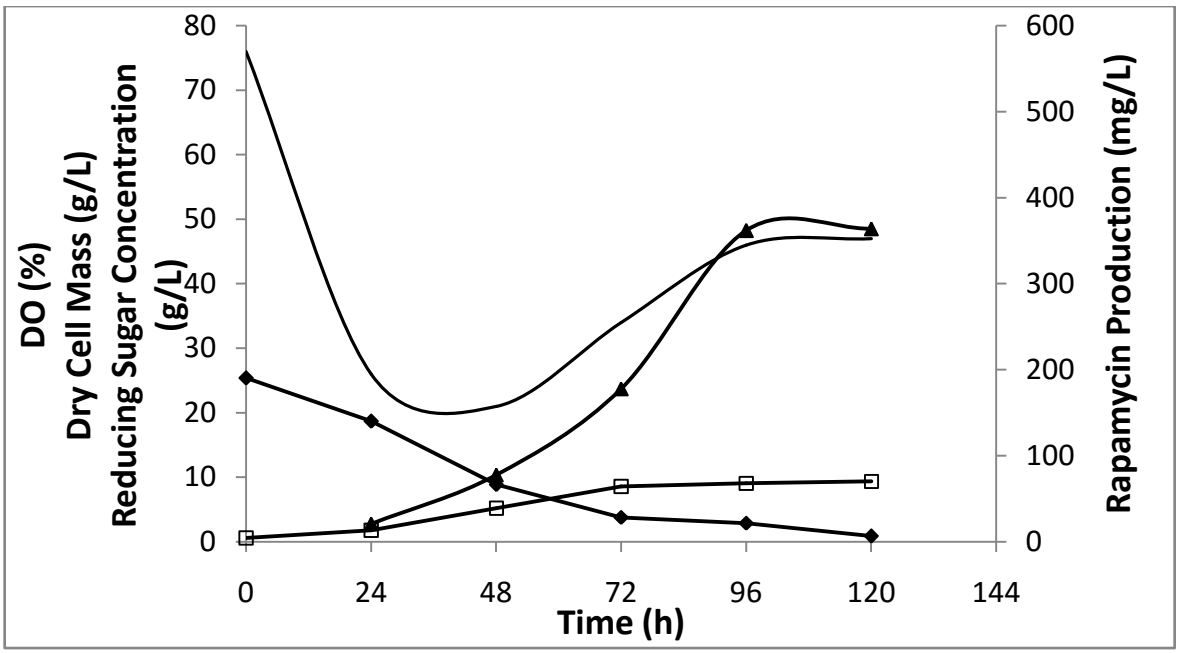

Fig 4.8 Variation of rapamycin production (Δ), dry cell mass (□), dissolved oxygen (-) and reducing sugar concentration (◊) with time at temperature 28 °C, 400 rpm, air flow rate 1 vvm

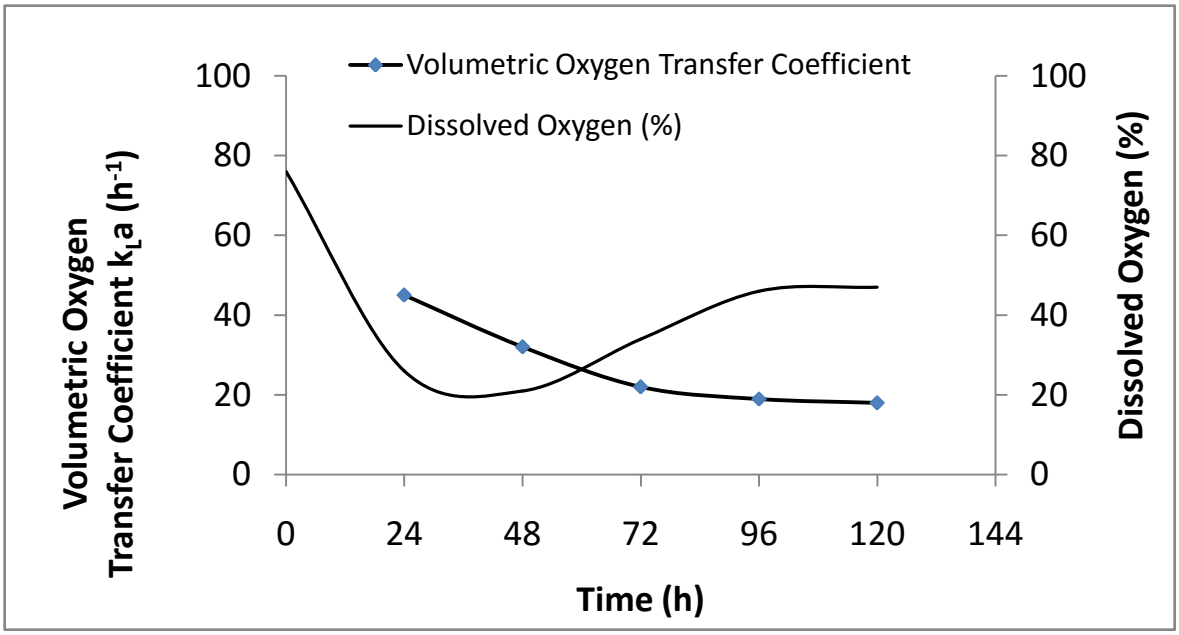

Fig 4.9: Variation of dissolved oxygen concentration (-) and volumetric oxygen transfer coefficient (k_La) (◊) with respect to time

4.2.4 Studies on broth rheology in 3L stirred tank reactor

The rheological variation in rapamycin fermentation broth was investigated. *Streptomyces* culture forms pellets as well as mycelia which affects the broth viscosity. Samples of fermentation broth were examined and the correlation between shear stress and shear rate at different time intervals was determined to establish the rheological behavior of the culture. Different rheological models were fitted into the shear stress and shear rate data at different time intervals to find out the most appropriate relation between the two. Fig 4.10 (A-D) shows the fitting of the data in different models viz. Casson Plastic, Power Law, Bingham Plastic and Newtonian model; and the fitness was evaluated in terms of coefficient of regression (R^2) value.

Based on the fitting of different models in rheological data of rapamycin production as shown in Fig 4.10 (A-D), parameters for each model were calculated and tabulated in Table 4.9. The values of regression coefficient for each model were also compared to evaluate the suitability of different models to the rheological data. It was found that the broth exhibited Newtonian behavior (R^2= 0.98) at the beginning of the fermentation while power law model was the best to describe the relation between shear stress and shear rate from 24 h to 120 h as shown in Table 4.9.

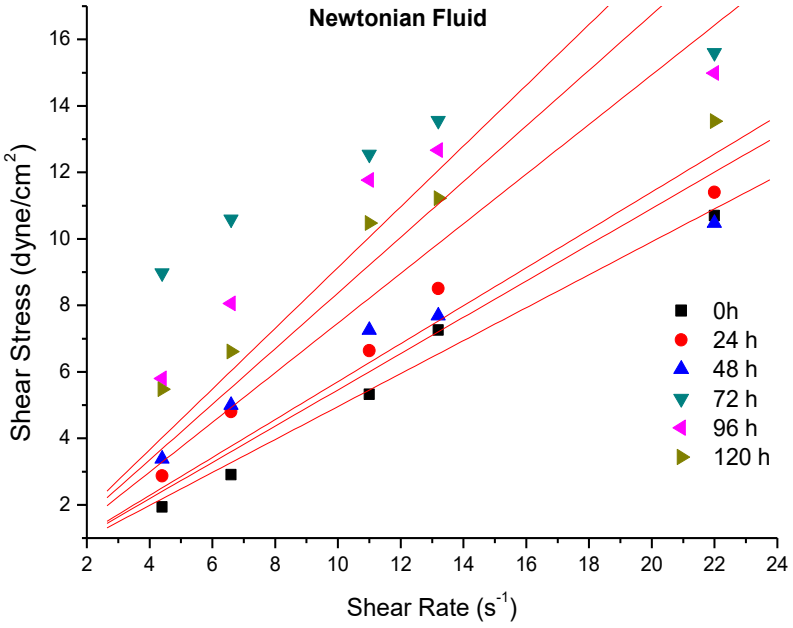

Fig 4.10 (A) Shear stress (τ) vs Shear rate (γ) for Newtonian Fluid Model

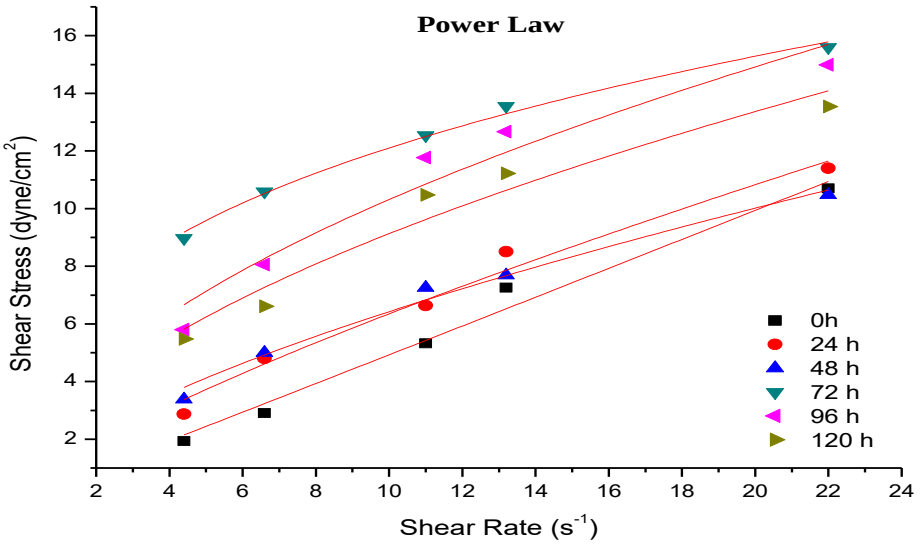

Fig 4.10 (B) Shear stress (τ) vs Shear rate (γ) for Power Law Model

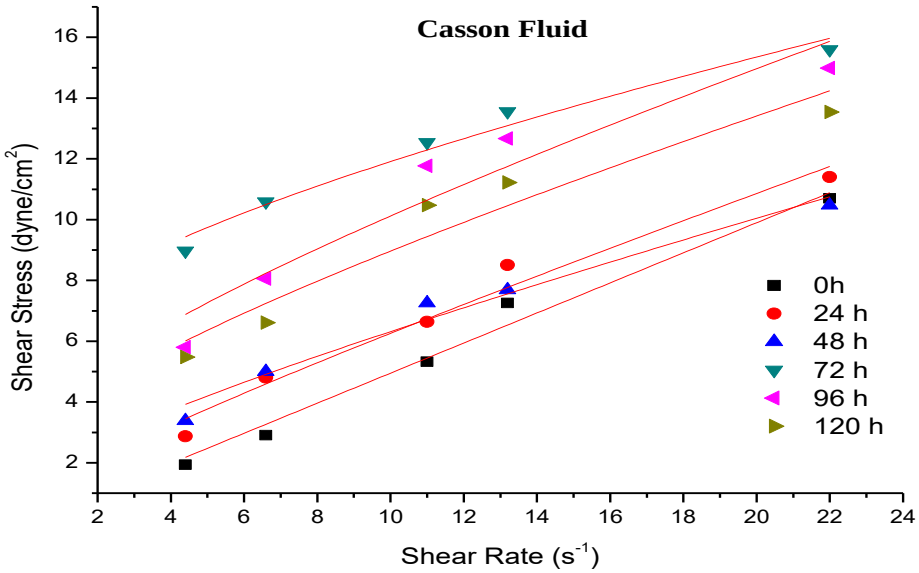

Fig 4.10 (C) Shear stress (τ) vs Shear rate (γ) for Casson Fluid Model

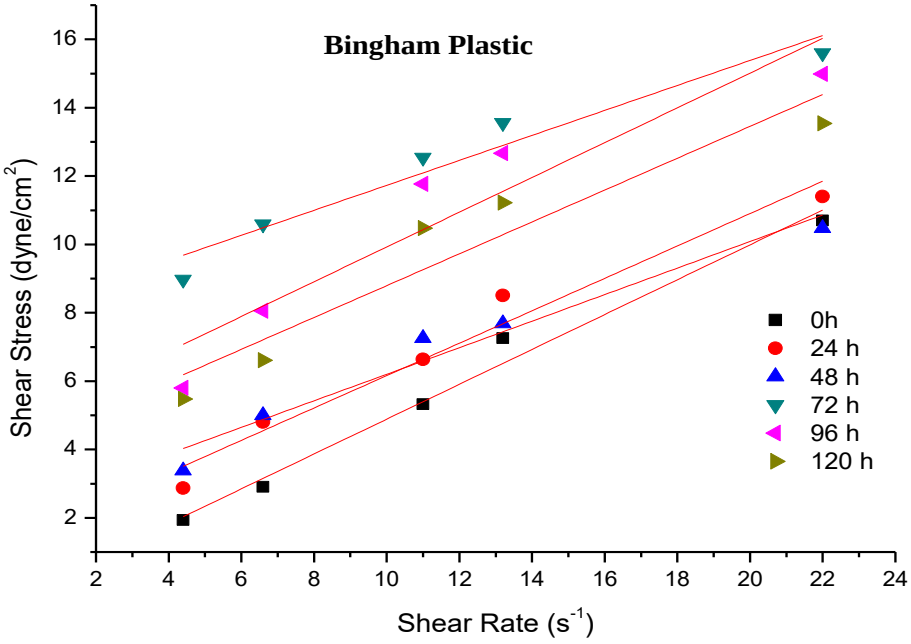

Fig 4.10 (D) Shear stress (τ) vs Shear rate (γ) for Bingham Plastic Model

The rheological behavior of broth has been found to be dependent on the age of fermentation process. Table 4.9 depicts the rheological data variation in reference to various models of broth characteristics. The power law model, exhibited the coefficient of regression (R^2) value from 0.936 to 0.992, whereas Bingham Plastic showed R^2 value from 0.859 to 0.958. Similarly, the regression coefficient for Casson plastic varied from 0.9 to 0.969 while the fitness of rheological data for Newtonian fluids was found to range from -1.79 to 0.985. Thus, the rheological data evaluation suggested that the broth followed Newtonian viscosity at the initiation of the process which was followed by Power Law model. This is also in line with other report [Pamboukian *et al.*, 2005]. Power law model has also been described earlier as the best suited model for other *Streptomyces* species for antibiotic production [Gavrilescu *et al.*, 1992].

Apparent viscosities (η_{app}) of fermentation broth were calculated at different shear rates and have been shown in Fig 4.11 which explains that the apparent viscosity increases with time upto 72 hours. As the trophophase ends, η_{app} tends to decrease which may be associated with the shear forces and the mycelium fragmentation. Moreover, the sporulation in the cells initiates as the ideophase begins. The variation of power law model parameters such as consistency index (k) and flow behavior index (n) and biomass concentration (x) with respect to time was studied. Fig 4.12 shows that during the batch fermentation, the consistency index increased up to 72 h when maximum biomass was produced. Maximum value of consistency index was found to be 5.576 dyne $s^n cm^{-2}$. The value of flow behavior index reduces upto 0.336 during 72 hours of fermentation. After 72 hours the consistency index reduced due to initiation of mycelial degradation. An increase in flow behavior index is noted towards the end of fermentation. It has been earlier reported that in case of

fermentation of mycelia forming microorganism the rheological properties vary during the course of fermentation. The correlations between the morphological behavior and rheological properties have been previously studied for cephalosporin C production [Gupta *et al.*, 2007, Mishra *et al.*, 2005].

The increase in mycelial growth also led to decrease in flow behavior index of the broth. The broth contained free mycelia as well as pellets which attributed to the increase in apparent viscosity of broth during the initial stages of fermentation. At later stages of the fermentation, the consistency index was found to decrease while the flow behavior index increased slightly. The dense mycelia of *S.hygroscopicus* ruptured as the fermentation advanced from growth phase towards stationary phase. At later stationary phase, the broth mainly consisted of aggregated mycelial clumps and pellets. This phenomenon could be attributed to the mycelial degradation due to prevalent shear forces in the fermentor. Similar observations have been noted in earlier studies [Riley *et al.*, 2000]. As the power law model best describes the rheological variation of fermentation broth, the residual plots for power law model fittings for different time intervals were evaluated. The residual plot shown in Fig 4.13 depicts that residual of shear stress are randomly distributed with respect to the independent variable which shows that model well defines the relation between the two.

Table 4.9: A comparative table of fitting viscosity data into different rheological models

(η : Newtonian viscosity; k: consistency index; n: flow behavior index; τ_o: Bingham Yield stress; K_p: Bingham viscosity; τ_c: Casson yield; K_c: Casson viscosity)

	Newtonian			**Power Law**			**Bingham Plastic**			**Casson Plastic**		
	$\tau = \eta * \gamma$			$\tau = k\gamma^n$			$\tau = \tau_o + K_p\gamma$			$\sqrt{\tau} = \sqrt{\tau_c} + K_c\sqrt{\gamma}$		
	(η: dyne s cm^{-2})			(k: dyne $s^n cm^{-2}$)			(τ_o: dyne cm^{-2})			(τ_c: dyne cm^{-2})		
				(n: dimensionless)			(K_p: dyne s cm^{-2})			(K_c: dyne s cm^{-2})		
Time (h)		Values	R^2		Values	R^2		Values	R^2		Values	R^2
0	η	0.495	0.985	k	0.479	0.979	τ_o	0.212	0.981	τ_c	0.002	0.979
				n	1.012		K_p	0.51		K_c	0.703	
24	η	0.570	0.917	k	1.078	0.985	τ_o	1.42	0.958	τ_c	0.344	0.968
				n	0.77		K_p	0.474		K_c	0.606	
48	η	0.545	0.759	k	1.469	0.982	τ_o	2.317	0.951	τ_c	0.86	0.969
				n	0.641		K_p	0.388		K_c	0.501	
72	η	0.913	-1.797	k	5.576	0.992	τ_o	8.074	0.929	τ_c	5.4	0.968
				n	0.336		K_p	0.365		K_c	0.356	
96	η	0.837	0.414	k	3.027	0.936	τ_o	4.838	0.859	τ_c	2.314	0.9
				n	0.532		K_p	0.509		K_c	0.525	
120	η	0.746	0.486	k	2.575	0.953	τ_o	4.133	0.883	τ_c	1.908	0.916
				n	0.549		K_p	0.466		K_c	0.509	

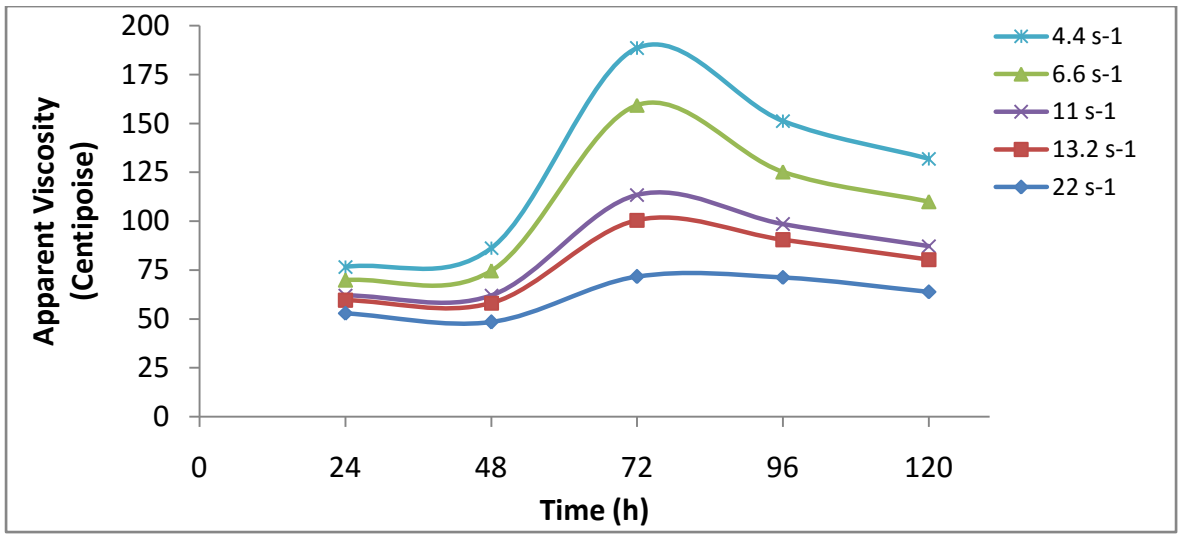

Fig 4.11 Variation of apparent viscosities with time at different shear rates

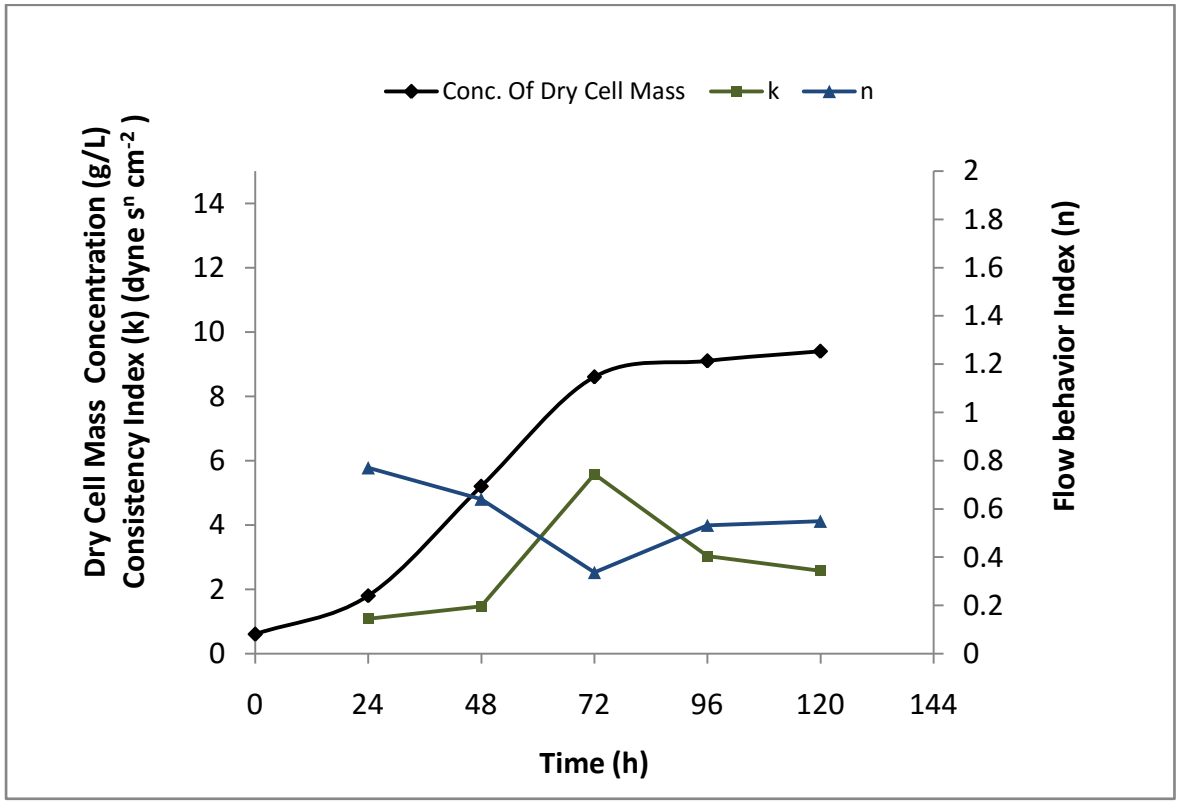

Fig 4.12 Comparison of flow behavior index (n) and consistency index (k) with variation in biomass concentration

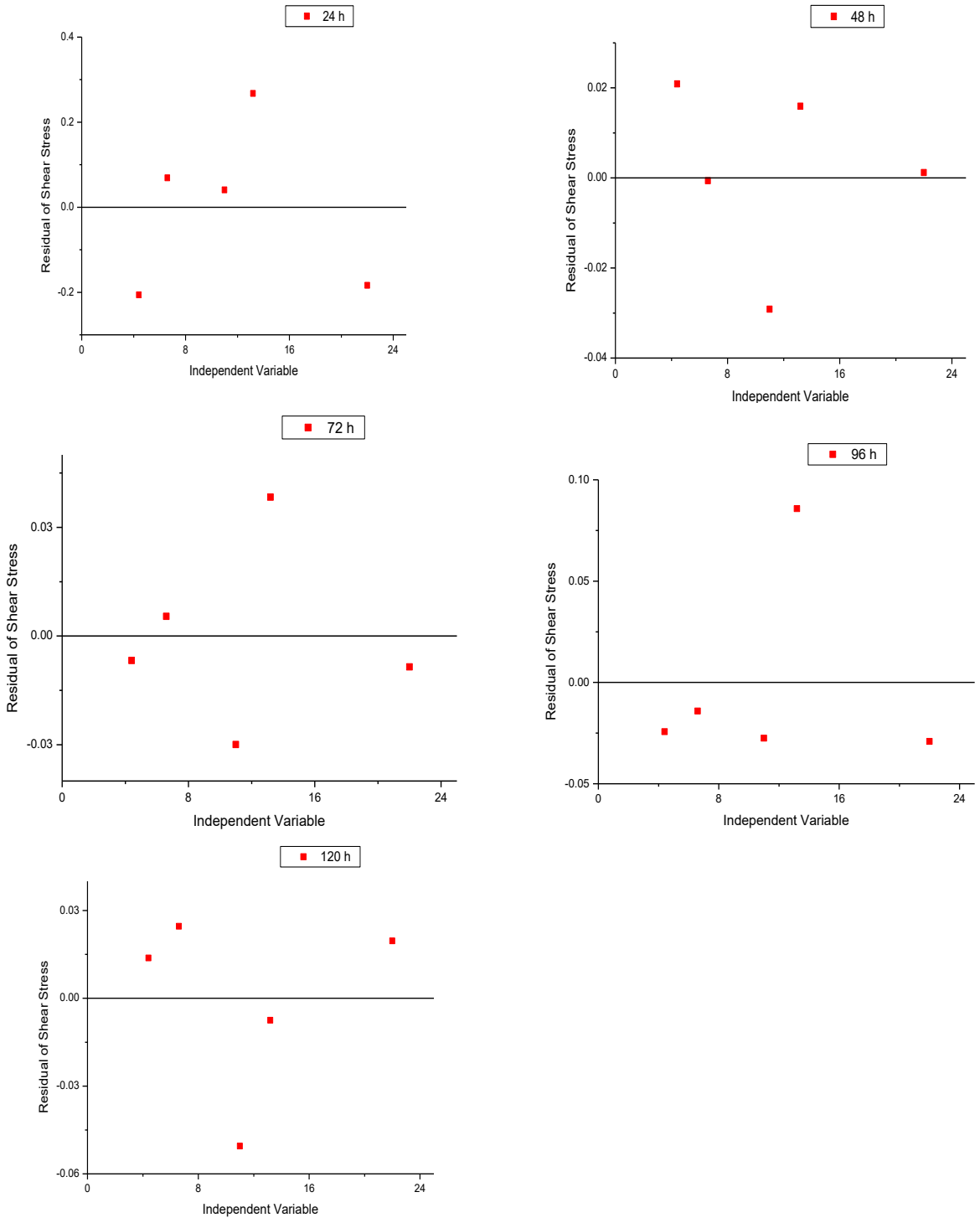

Fig 4.13: Plot of Residual Shear Stress vs independent variable at 24, 48, 72, 96 and 120 h.

4.3 Different strategies for rapamycin production

Based on the optimization and production studies conducted in shake flask and stirred tank reactor attempts were made to enhance the production of rapamycin.

The selection of the strategies was done on the basis of different parameters which have been earlier reported to effect antibiotic production as listed in the table 4.10.

Table 4.10 Strategies for production of rapamycin

S.No.	Strategies	Production parameter
1	Immobilization of *S. hygroscopicus* using different carriers	Reuse of cells
2	Production of rapamycin in an Air Lift Reactor	Dissolved oxygen concentration
3	Co-culture of *S. hygroscopicus* with a competitor strain	Stress condition
4	Pulse feeding strategy for rapamycin production	Extension of stationary phase

Strategies for production of rapamycin were evaluated and their effects on product concentration have been discussed in the subsequent sections.

4.3.1 Immobilization of *S. hygroscopicus* using different carriers

Streptomyces hygroscopicus was immobilized using different carriers and the effect of immobilization on rapamycin production was analyzed. Carriers were selected on the basis of ease of availability, non-toxic to microbial growth and ability to withstand autoclave conditions. These carriers included Polyurethane foam (PUF), Sintered beads (also known as Siran bead), Glass beads and Corn peanuts. These carriers varied in their property such as porosity, composition and particle size. The pre-treatment of the carriers were carried out which were then subjected to immobilization. Immobilized cell-carrier system was then transferred to 250 mL shake flask each containing 50 mL of fermentation medium.

4.3.1.1 Growth of *S. hygroscopicus* on different carriers

Four different carriers were used for immobilization study and depending on their properties such as porosity, charge, composition and particle size. Different amount of biomass were immobilized as shown by the Fig 4.14. Immobilized biomass was calculated in terms of weight of *S. hygroscopicus* immobilized per unit weight of carriers. It is clearly observed that maximum immobilization of 0.84 g/g of carrier is observed in PUF as they have very high porosity (approximately 94%) and least was shown by glass beads with minimum porosity out of the for carriers used. Hence, maximum immobilization (cells per unit weight of carrier) was observed in case of PUF and minimum in case of glass beads as shown in Fig. 4.14. Sintered beads and foam peanuts exhibited intermittent immobilization capacity

.**Scanning Electron microscopy of immobilized carriers**

The immobilized carriers were observed by Scanning Electron microscope (Evo 18 Research, Zeiss SEM after coating with gold particles by Q 150R ES Qourum) at Central Instrument Facility Centre (CIFC), IIT (BHU) Varanasi. Fig 4.15, clearly shows the immobilization results and verifies that PUF cubes had maximum immobilization as a uniform layer of mycelial film is formed. Microscopic view of siran beads and peanut foam cubes showed dense immobilization whereas most sparse growth was observed in glass beads having scattered growth of cells.

4.3.1.2 Study of release of cells by immobilized carriers during production

Cell release study was carried out to study the robustness of the immobilization of cells. Cell release during the fermentation was determined using samples withdrawn at regular interval from the fermentation broth. The percentage of cell release was calculated using eq. 4.3.1.

$$Percentage\ of\ cell\ release = \frac{\text{weight of dry cell mass released per unit weight of carriers}}{\text{weight of dry cell mass immobilized by unit weight of carriers}} \times 100 \qquad \text{-(4.3.1)}$$

Cell release study was used to determine the loss of immobilized biomass into the broth. Fig 4.16 shows the cell release percentage in different carriers. Maximum cell release was observed in case of glass beads owing to its lower porosity. Cells were adsorbed onto the surface of the glass beads which were mostly released during agitation at 200 rpm. While, minimum cell release was exhibited by siran beads due to its smaller pore size. Foam peanuts and PUF showed intermittent features as their pore size were larger than siran beads.

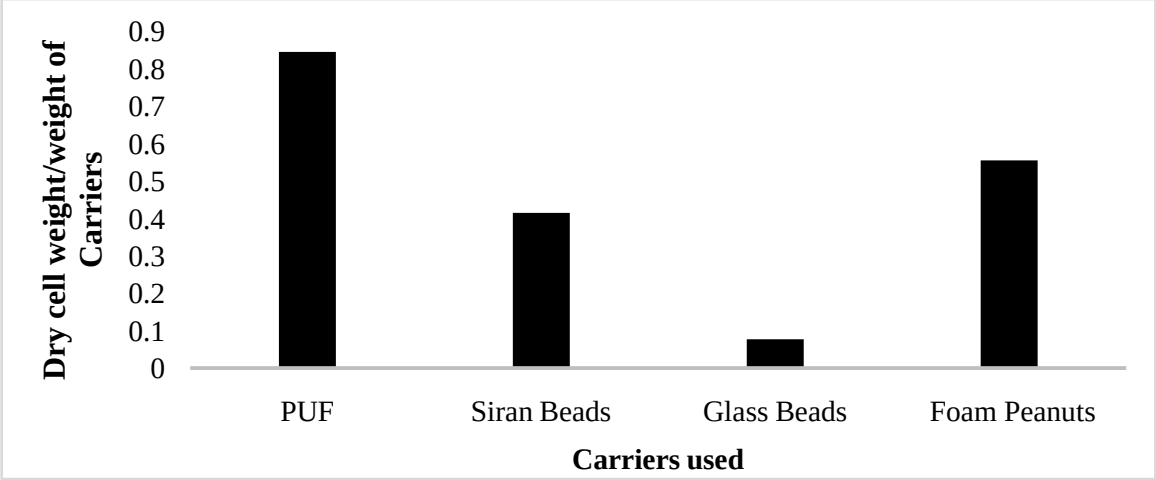

Fig 4.14 Variation of dry cell weight of *S. hygroscopicus* per unit weight of different carriers

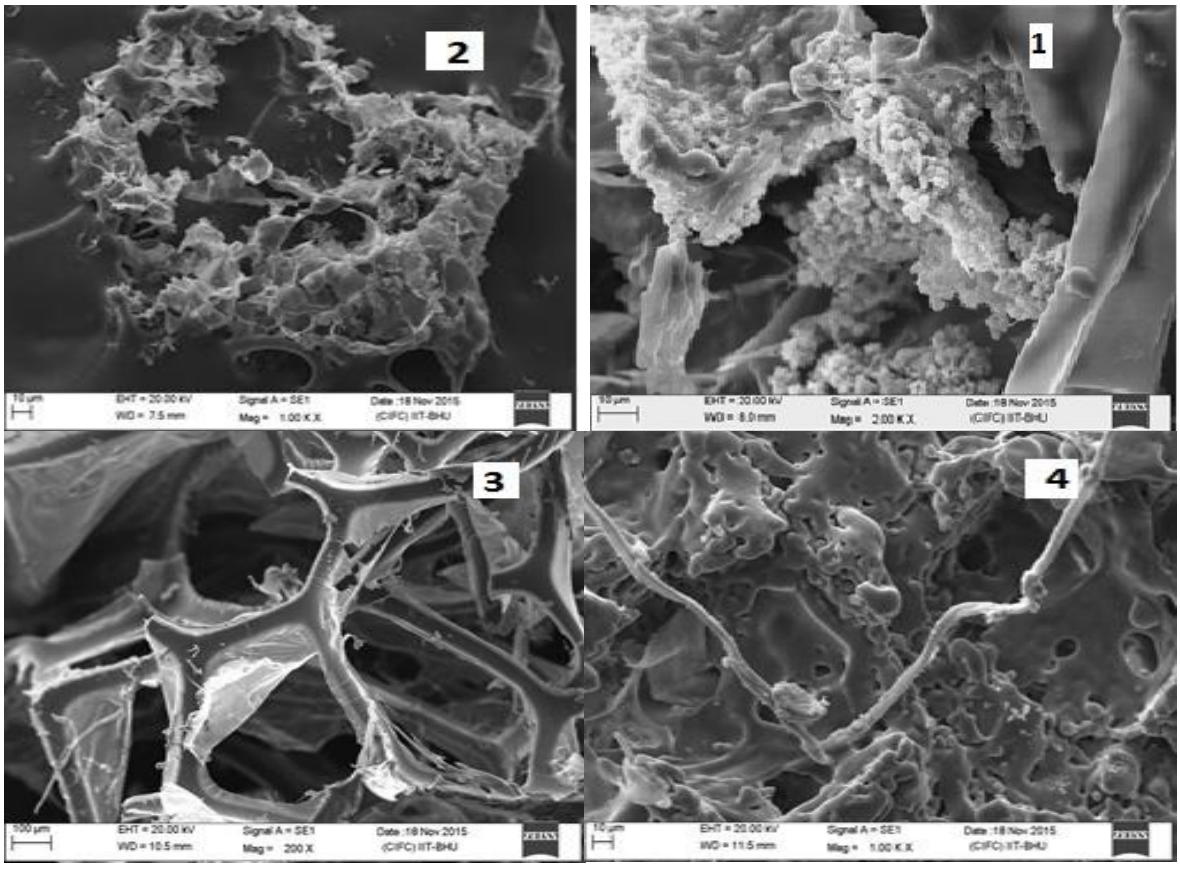

Fig 4.15 SEM image of different immobilized carriers
1: Foam peanuts 2: Glass Beads 3: PUF 4: Siran Beads

4.3.1.3 Production of rapamycin using different carriers for immobilization

Fermentation was carried out in four different immobilized systems and the samples were collected at regular intervals to analyze the concentration of rapamycin produced in the broth. Fig 4.17 shows the concentration of rapamycin produced in different immobilized fermentation system after 96 hours of production of rapamycin. It was observed that maximum production of rapamycin occurred when *S.hygroscopicus* were immobilized on PUF cubes.

Production was calculated in terms of weight of rapamycin produced per unit weight of carriers as shown in Fig 4.17. It was determined that though maximum production per unit weight was observed in PUF carriers but minimum was observed in glass beads. This could be correlated to the SEM studies which suggest uniform distribution of cells on the PUF carriers which may lead to lower mass transfer limitation. Other workers have also reported PUF as one of the suitable carriers for immobilization owing to their high porosity and inert nature [Kattimani *et al.*, 2009, Zhu *et al.*, 2015].

4.3.1.5 Production of rapamycin by *S.hygroscopicus* immobilized on PUF for repeated batches

The process of production of rapamycin on different carriers was evaluated for repeated batch cycles. The production was analyzed for five different cycles and the corresponding cell release percentage was calculated. The cell release percentage was based on initial cell mass of the immobilized PUF cubes in the first cycle. Fig 4.18 suggests that the product concentration was consistent for three cycles of fermentation while after the fourth cycle rapamycin concentration decreased significantly from 248 mg/L to 197 mg/L.

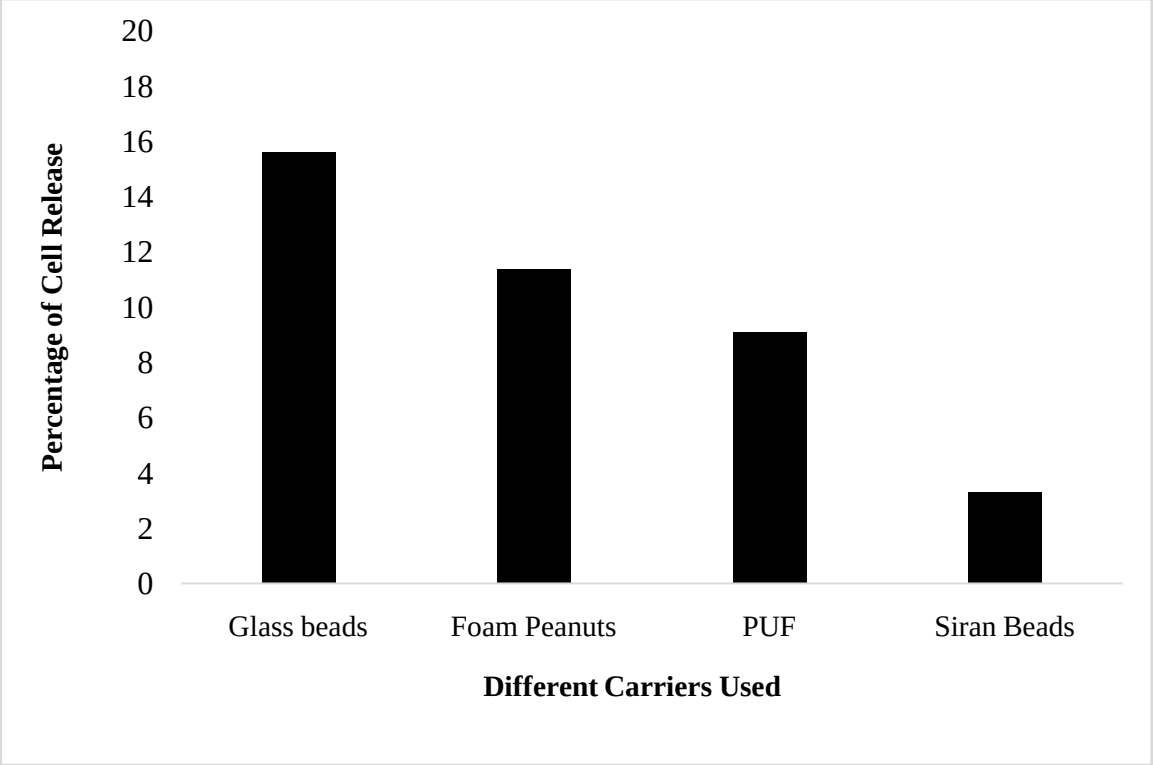

Fig 4.16 Cell Release Study in different immobilized systems

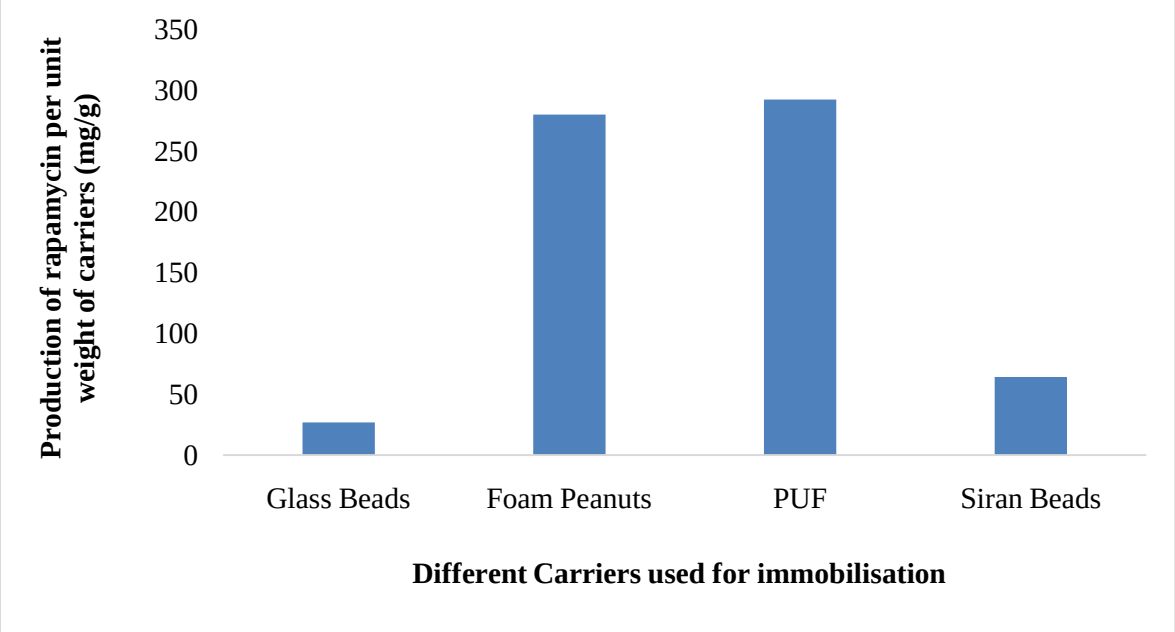

Fig 4.17 Production of rapamycin in different immobilized carriers

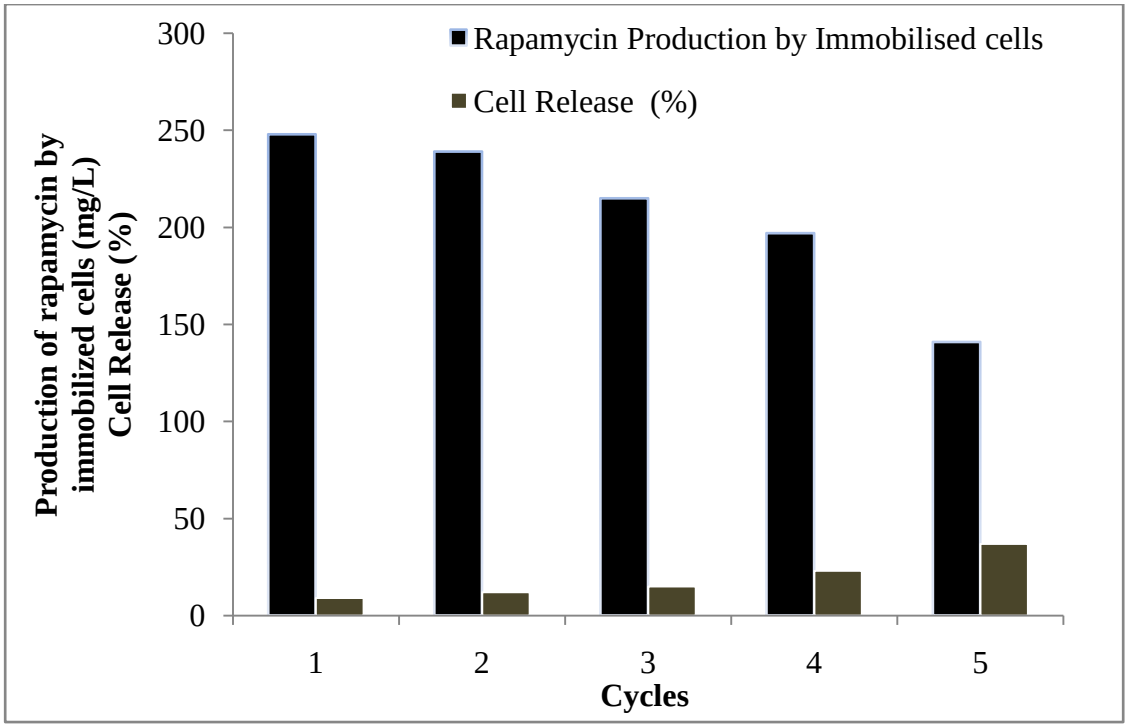

Fig 4.18 Rapamycin production and cell release during repeated batch fermentation using *S.hygroscopicus* immobilized on PUF.

4.3.2 Study of rapamycin production in an internal loop airlift bioreactor

Airlift bioreactor provides an alternative to the conventional stirred tank reactor being designed for less shear forces and adequate ability of mass transfer [Garcia-Ochoa *et al.*, 2009, Schügerl, 1990]. It has been well established that rate of oxygen transfer affects the product formation by filamentous microorganism in submerged culture. Moreover, it has been earlier found that rapamycin production is improved by high dissolved oxygen supply [Yen *et al.*, 2013]. An early study based on determination of fate of carbon, hydrogen and oxygen atoms in antibiotic biosynthesis using isotope labeling explained the importance of atmospheric oxygen. According to this study, $^{18}O_2$ labeled atmospheric oxygen was found to get incorporated into the polyketide structure of aspyrone [Simpson, 1998].

Therefore, rapamycin production was studied in airlift bioreactor and kinetic analysis was done. A 3L indigenously designed borosilicate airlift reactor was used with aspect ratio as 10 and area of riser to downcomer was 1.042. The dimensions were suitable for autoclaving. The bioreactor was placed inside a closed chamber which was fumigated as well as sterilized using ultra violet radiations.

Fig 4.19 details the set up of airlift reactor facilitated with aseptic transfer of medium and samples by using peristaltic pumps. Fermentation conditions were kept same as that of stirred tank reactor having temperature maintained at 28°C and pH 6.0. Aeration parameter was optimized for maximum production of rapamycin.

Fig 4.19 Fermentation set up of internal loop ALR

4.3.2.1 Variation of rapamycin production at different aeration rates

Rapamycin production was carried out at different aeration rates. The variations of gas hold up and product concentration was evaluated at different aeration rated. Fig 4.20 shows the variation of gas hold up at different superficial gas velocities. The result shown in Fig 4.20 depicts that as the fermentation age increases, the value of gas hold up tends to decrease such that at 120 hours the gas hold up reduces by about 20% at superficial gas velocity of 0.081 ms^{-1}. The production of rapamycin was also affected by different aeration rates in the ALR. Fig 4.21 illustrates the dependence of rapamycin production on aeration rates in an internal loop airlift reactor. The aeration rate was calculated in vvm (volume of air per unit volume of reactor per minute) and was controlled using a rotameter. It was observed that rapamycin concentration increased when aeration rate was increased from 0.5 vvm to 1.5 vvm and reached 391 mg/L. No significant change was observed on further increase in aeration rate. Thus, 1.5 vvm was the optimum aeration rate for rapamycin production and used for further studies.

4.3.2.2 Rapamycin production, biomass generation and substrate depletion

Batch production of rapamycin was carried out in 3L airlift reactor. Fig 4.22 shows rapamycin production, biomass and reducing sugar concentration during fermentation process. Concentration of biomass increased up to 72 hours after which the cells entered into the stationary phase. The reducing sugar concentration decreased by 84.4% of its initial amount as the cells enter the ideophase. Rapamycin production was measured from 24 hours of fermentation and was found to reach its maximum value in 96 hours. Production of rapamycin was higher in airlift reactor compared to stirred tank reactor by 8%. Thus,

comparable production was obtained in stirred tank reactor and airlift reactor when operated at aeration rates of 1.0 vvm and 1.5 vvm respectively.

4.3.2.3 Determination of kinetic parameters for rapamycin production in ALR

Efficiency of airlift reactor for production of rapamycin was evaluated by calculating the kinetic parameters. Fig 4.23 shows the variation of specific growth rate and specific product formation rate with fermentation time. The variation of product formation rate with time shows that it is a mixed type of product. It was found that specific maximum specific product formation rate was achieved during 72 hours after which it reduced significantly whereas maximum specific growth rate of 0.076 h^{-1} was achieved at 24 hours. Maximum product concentration was found at 96 hours beyond which there was no significant increase. Table 4.11 shows the result of kinetic analysis which included the yield of the process, maximum specific growth rate and specific product formation rate. The table compares the kinetic parameters of rapamycin production in ALR and STR.

It can be observed that dry cell mass concentration was higher in case of airlift reactor as compared to stirred tank reactor. The maximum specific growth rate was 0.076 h^{-1} which was higher than observed in the mechanically agitated reactor. Higher growth rate could be associated with the fact that there is absence of shearing forces in airlift reactor. Similar results have been reported in earlier studies [Saravanan *et al.*, 2008], where specific growth rate was found to be higher in case of ALR as compared to STR. Rapamycin concentration in ALR was 391 mg/L which was higher as compared to stirred tank reactor. Maximum specific product formation rates were similar in ALR and STR. The product yield in ALR was 44.9 mg rapamycin/g of dry cell mass which was higher as compared to STR.

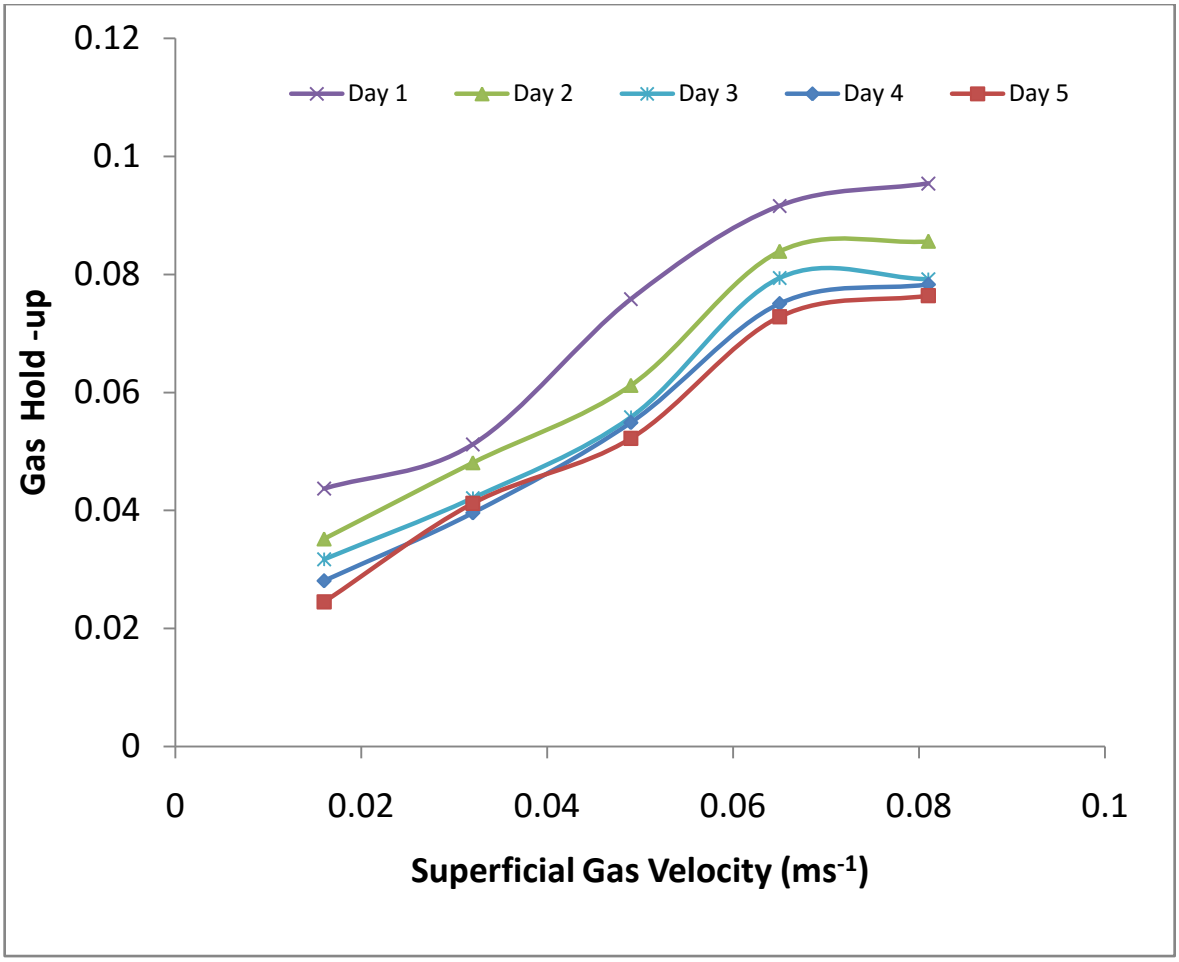

Fig 4.20 Variation of gas hold up at different gas velocities

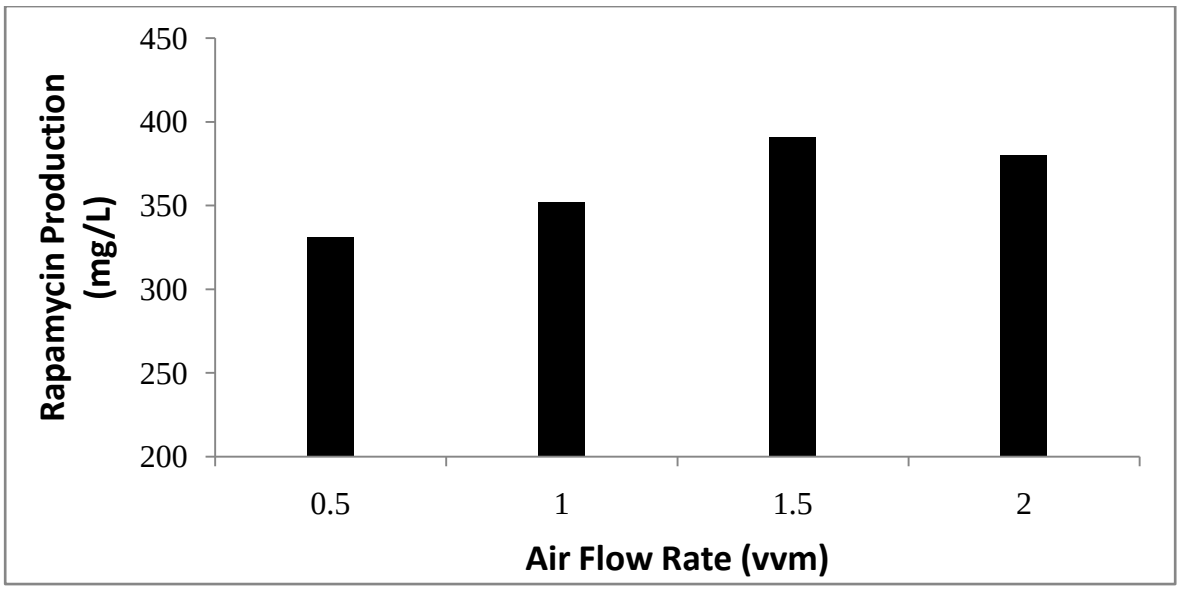

Fig 4.21 Variation of rapamycin concentration with aeration rate in an internal loop airlift reactor

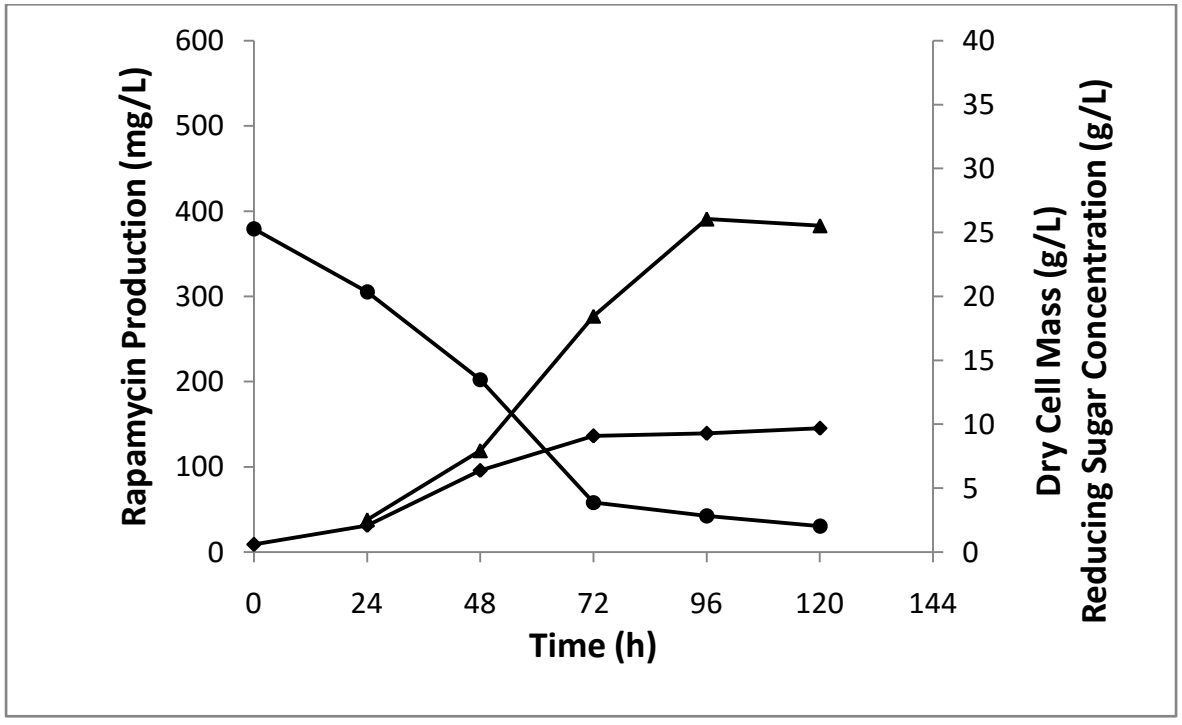

Fig 4.22 Variation of Rapamycin production (filled Δ), dry cell mass (filled ◊) and reducing sugar concentration (filled ○) with time during batch production of rapamycin in air lift reactor.

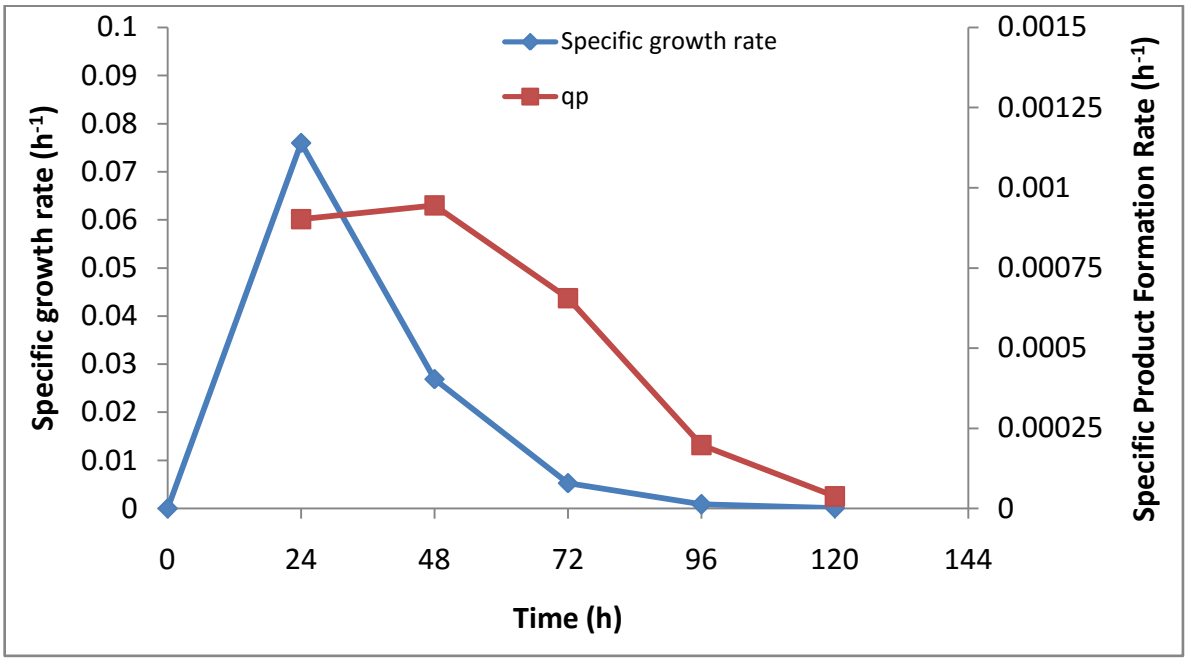

Fig 4.23 Variation of specific growth rate (μ) and specific product formation rate (q_p) in an ALR

Table 4.11: Comparison of kinetic parameters for rapamycin production in ALR and STR

	Maximum specific growth rate (μ)	Maximum Product Concentration	Dry cell mass yield ($Y_{x/s}$)	Product yield per unit biomass ($Y_{p/x}$)	Specific product formation rate (q_p)
	(h^{-1})	(mg/L)	(g/g)	(mg/g)	(mg/g/h)
ALR	$0.076\pm6\times10^{-4}$	391±3.1	0.39±0.003	44.9±0.35	0.46±0.017
STR	$0.07\pm8\times10^{-4}$	364±4.8	0.36±0.007	41.3±0.44	0.33±0.009

4.3.2.4 Estimation of dissolved oxygen concentration for rapamycin production in ALR

The variation in dissolved oxygen (DO) concentration and corresponding volumetric oxygen transfer rate (k_La) during rapamycin production in ALR was studied. Fig 4.24 shows that dissolved oxygen concentration decreased up to 48 hours and then started increasing. As the cells enter the stationary phase after 72 hours, the DO concentration increased and reached a constant value.

k_La was found to decrease with time upto 72 hours and then became constant. k_La was found to be 26 h^{-1} at the end of fermentation. It was observed that higher k_La was achieved in ALR as compared to STR as the final value of STR was 18 h^{-1}**.** Better oxygen transfer ability of ALR could be the reason for higher specific growth rate and higher rapamycin concentration. Literature suggests that impeller flooding causes reduced oxygen transfer efficiency in stirred tank reactors [Lueske *et al.*, 2015]. The results obtained from ALR studies shows that comparative yield of rapamycin could be obtained by using the pneumatic bioreactor.

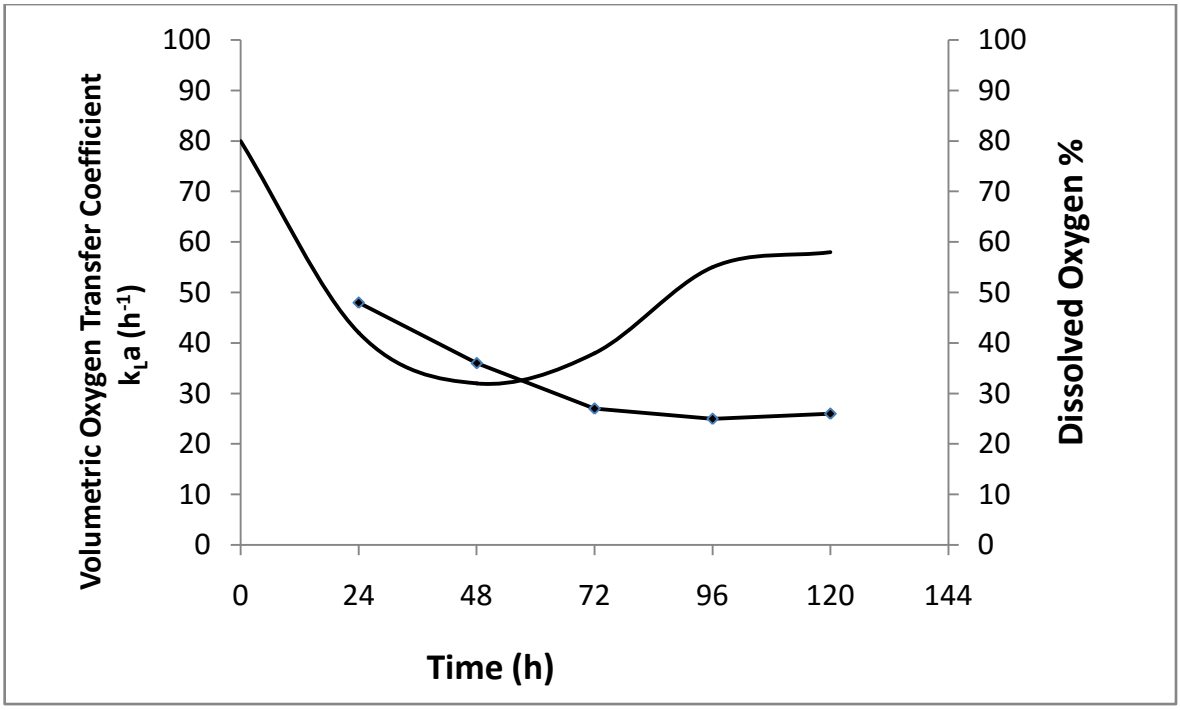

Fig 4.24 Variation in dissolved oxygen concentration (-) and k_La (filled ◊) during batch production of rapamycin in airlift reactor

4.3.3 Study of rapamycin production when *S.hygroscopicus* was grown with a competitor strain

Antifungal activity of rapamycin against *Candida albicans* NCIM 3471 has been employed in the present study to analyze the effect on the production of rapamycin by mimicking the natural condition of co-existence of the two competitors. *Streptomyces hygroscopicus* was co-cultured with *Candida albicans* against which it exhibits antifungal activity in the medium.

4.3.3.1 Adaptation of *S.hygroscopicus* for growth in co-culture condition

Streptomyces hygroscopicus was grown for three generations on solid MGYP media in vicinity to its competitive strain *Candida albicans* NCIM 3471. Fig 4.25 shows the result of agar plates streaked with *S.hygroscopicus* and *C.albicans*. For every successive step, a loopful of culture of *S.hygroscopicus* was carefully collected from the previous step and streaked on the next plate. Culture of *C.albicans* was streaked at the centre.

A loopful culture of *Streptomyces hygroscopicus* growing in the vicinity of *C.albicans* from step 3 was collected and transferred to MGYP liquid medium, pH 6.0 and temperature 28°C. The 10% inoculum from the seed culture was then transferred to the production medium.

Fig 4.25 Co-cultured plates of *S.hygroscopicus* and *C.albicans*

4.3.3.2 Study for optimization of inoculum size of *C.albicans*

Production of rapamycin was studied in the optimized production medium containing 10% of *S.hygroscopicus* and varying initial concentration of *C.albicans*. Culture of *C.albicans* used for the study was grown in MGYP medium till the final concentration reached about 10^5 cells/ mL. Fig 4.26 shows the variation of rapamycin production due to change in inoculum concentration of *C.albicans.*

It was observed that as the inoculum size of *C.albicans* was increased to 3% (v/v), rapamycin production increased upto 348 mg/L in shake flask culture. However, no rise in rapamycin concentration was noticed as the concentration of the competitor strain was increased further. This could be the result of shortage of substrate availability which could affect either growth of *S.hygroscopicus* or rapamycin production or both. Thus, 3% of *C.albicans* was found to be the optimum inoculum size for rapamycin production.

4.3.3.3 Study for optimization of inoculation time

Study was carried out to evaluate the effect of different inoculation time of the competitor strain on rapamycin production. Fig 4.27 shows that the effect of time of introduction of the competitive strain on rapamycin production was significant.

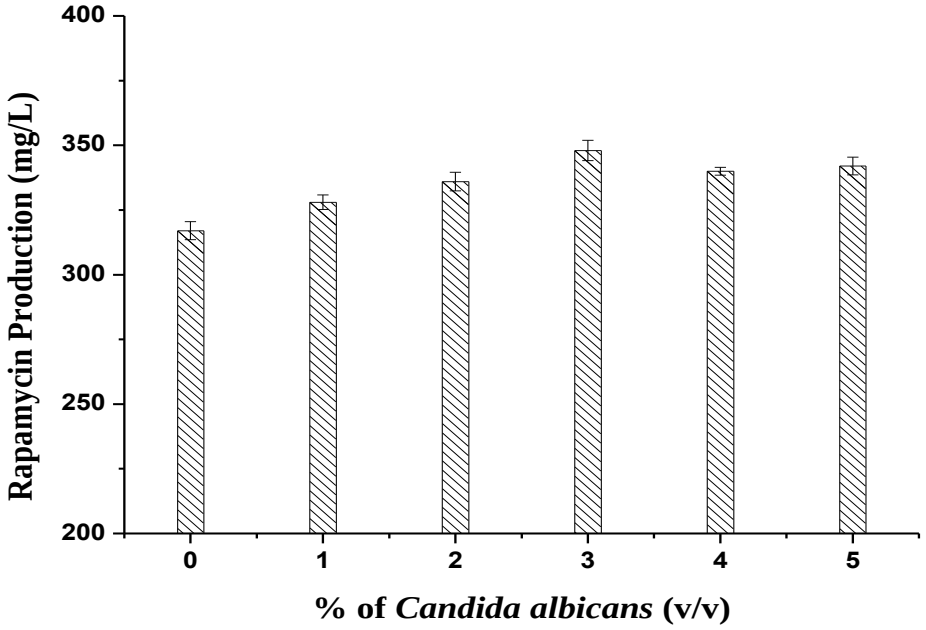

Fig 4.26 Variation in rapamycin production with different inoculum size of *C.albicans* in the co-culture study

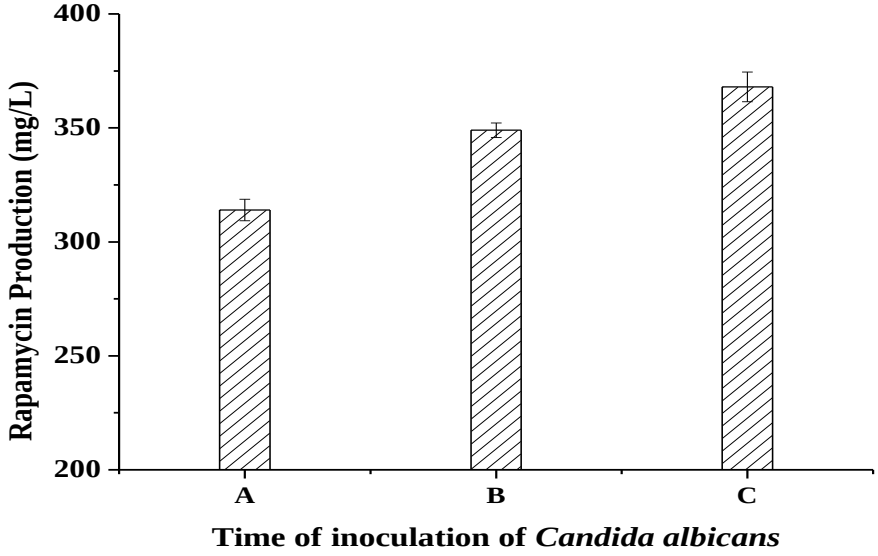

Fig 4.27 Effect of time of inoculation of *C.albicans* on rapamycin production in co-culture
A: 24 hours before inoculating *S.hygroscopicus*
B: Inoculating concurrently with *S.hygroscopicus*
C: 24 hours after inoculating *S.hygroscopicus*

When 3% *C.albicans* was inoculated 24 hours before inoculation of *S.hygroscopicus*, the production of rapamycin was 314 mg/L which was significantly less than co-inoculation of the two species. Moreover, the production of rapamycin increased upto 368 mg/L when *C.albicans* was inoculated after 24 hours of inoculation of *S.hygroscopicus.* This result could be related to the fact that *S.hygroscopicus* could adapt to the environment and production of the antibiotic initiated when the competitor strain was introduced, which further triggered the production. Recent report suggest that *Streptomyces* sp. are capable of secreting volatile organic compounds (VOCs) such as trimethyl amine (TMA) when there is a fungal interaction which enhances microbial competition and increases antibiotic production [Jones *et al.*, 2017]. Other workers have also reported the elicitation of secondary metabolite production in co-culture conditions [Ola *et al.*, 2013, Trischman *et al.*, 2004]. Thus, the production of rapamycin can be carried out in co-culture condition at higher scale.

4.3.4 Fed batch fermentation strategy using pulse feeding

A fed batch strategy for rapamycin production was evaluated based on previous batch fermentation kinetics. The study was carried out in stirred tank reactor as both ALR and STR showed comparable results. It was noted earlier, in batch fermentation studies that the production of rapamycin was significant up to 96 hours and at initial mannose concentration of 25 g/L (Fig 4.8). Thus, a strategy was adopted such that, two pulse feed of 50 mL each were provided to the 2L fermentation broth. One feed contained the precursors sodium acetate and sodium propionate at a concentration of 20 g/L. These precursors could not be added in batch culture as they tend to inhibit the growth of cells. For the second

feeding, mannose was used at a concentration required to maintain the cells at stationary phase. This concentration was based on the maintenance energy calculated in the earlier experiments when the initial concentration of mannose was kept as 25 g/L.

4.3.4.1 Study of fed-batch fermentation parameters

Fed- batch fermentation for rapamycin production was carried out for 168 h when the dry cell mass concentration reached 9.5 g/L (Fig 4.28). The feed1 was provided at 72 hours when the DO concentration reached 40% level. Then, at 96 hours, the reducing sugar concentration at was below 3g/L. Thus, based on reducing sugar concentration requirement for cellular maintenance for next 48 hours, the mannose concentration was maintained at 3 g/L.

Rapamycin concentration continued to increase upto 481 mg/L after 144 hours of fermentation beyond which there was no significant enhancement in rapamycin production. This may be due to other factors becoming limiting. Similar results were obtained by Elsayed *et al.,* when they obtained higher yield of oxytetracycline production in fed –batch cultivation carried out using mono substrate feeding compared to complete medium feeding [Elsayed *et al.*, 2015].

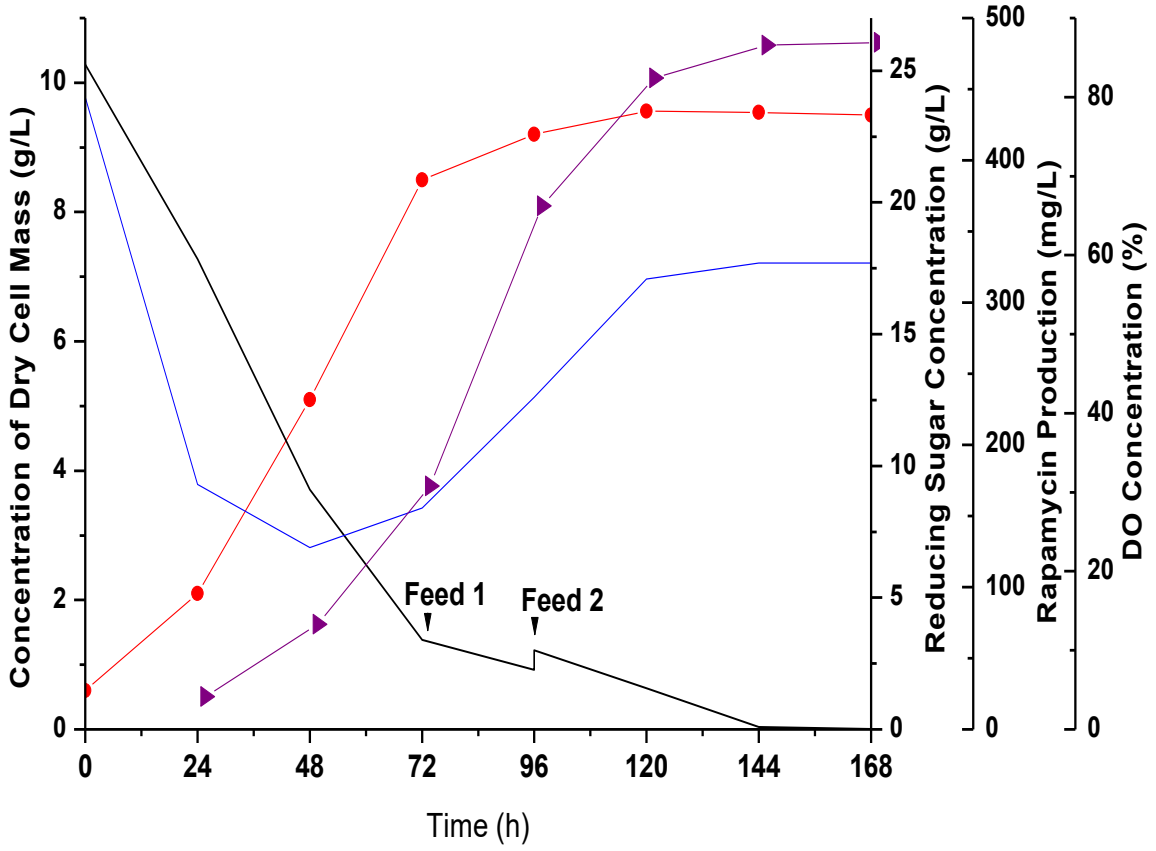

Fig 4.28: Fed- batch profile for rapamycin production based on pulse- feeding (substrate and precursors). Concentration of dry cell mass (◊); concentration of rapamycin (Δ); Concentration of reducing sugar (black _); DO concentration (blue ___)

4.3.4.2 Evaluation of fed batch kinetics

The fed batch feeding strategy was evaluated on the basis on kinetics of cell growth and product formation. The variations of growth rate and product formation rate with time were determined. It was found that (Fig. 4.29) that maximum value of growth rate was reached in about 48 hours which was reduced gradually. While the maximum value of product formation rate was reached at about 72 hours. Later, though rapamycin formation rate decreased but production was evident till 144 hours which led to accumulation of product and higher concentration was reached as compared to batch fermentation. The fed-batch strategy led to 32% enhancement in rapamycin production when compared to the batch fermentation.

The result of enhanced production can be supported by an earlier study which suggests that slow feeding of carbon source can lead to enhancement in polyene macrolide production and increased maturation time [Martin *et al.*, 1975]. Candidin and candihexin production has been enhanced due to increased polyene production rate by slow glucose feeding which led to slower transition from trophophase to ideophase [Martin *et al.*, 1975]. Rapamycin is also a polyene macrolide.

The comparison of kinetic parameters has been shown in Table 4.12 where fed batch fermentation was found to be an efficient process.

Pulse feeding strategy led to enhanced productivity as well as product yield. This strategy could be implemented in ALR also.

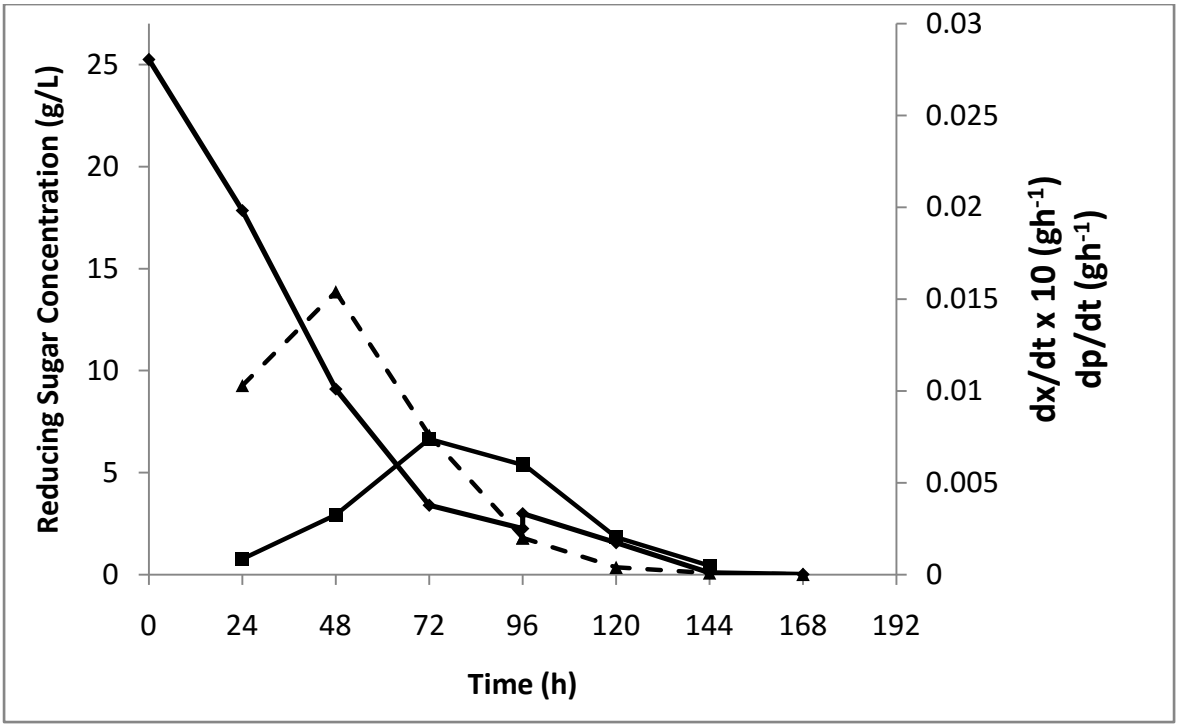

Fig 4.29: Variation of pulse feeding on growth rate (dx/dt) and product formation rate (dp/dt) during fed-batch fermentation: Reducing sugar concentration (◊); dx/dt (filled Δ); dp/dt(filled □)

Table 4.12: Kinetic parameters for rapamycin production in fed- batch mode

	Maximum Product Concentration (mg/L)	Product yield per unit biomass ($Y_{p/x}$) (mg/g)	Specific product formation rate (q_p) (mg/g/h)	Productivity (mg L^{-1} h^{-1})
Fed- batch	483	54.26	0.35	3.34
Batch	364	41.3	0.33	3.03

4.3.4.3 Study of broth rheology during fed-batch fermentation

The comparison of broth rheology for batch and fed- batch fermentation shows there is a correlation between the biomass growth and consistency index. Fig 4.30 shows that in fed-batch fermentation, a pulse feeding strategy led to maintenance of sub-maximal growth rate which resulted in cellular growth upto about 72 of fermentation. The consistency index increased significantly upto 5.39 dyne s^n cm^{-2} at 72 h. Further, addition of substrate at 96 h did not increase the k value. The flow behavior index decreased upto 72 h after which a slight increment was noted.

Previous study shows that a strong correlation exists between biomass concentration and consistency index. A decrease in the consistency index is noted due to degradation of mycelia [Pollard *et al.*, 2002]. The study of rheological variation of the broth with time can be significant as it provides an insight into the parameters affecting the mass transfer which in turn can affect rapamycin production [Blanch *et al.*, 1976].

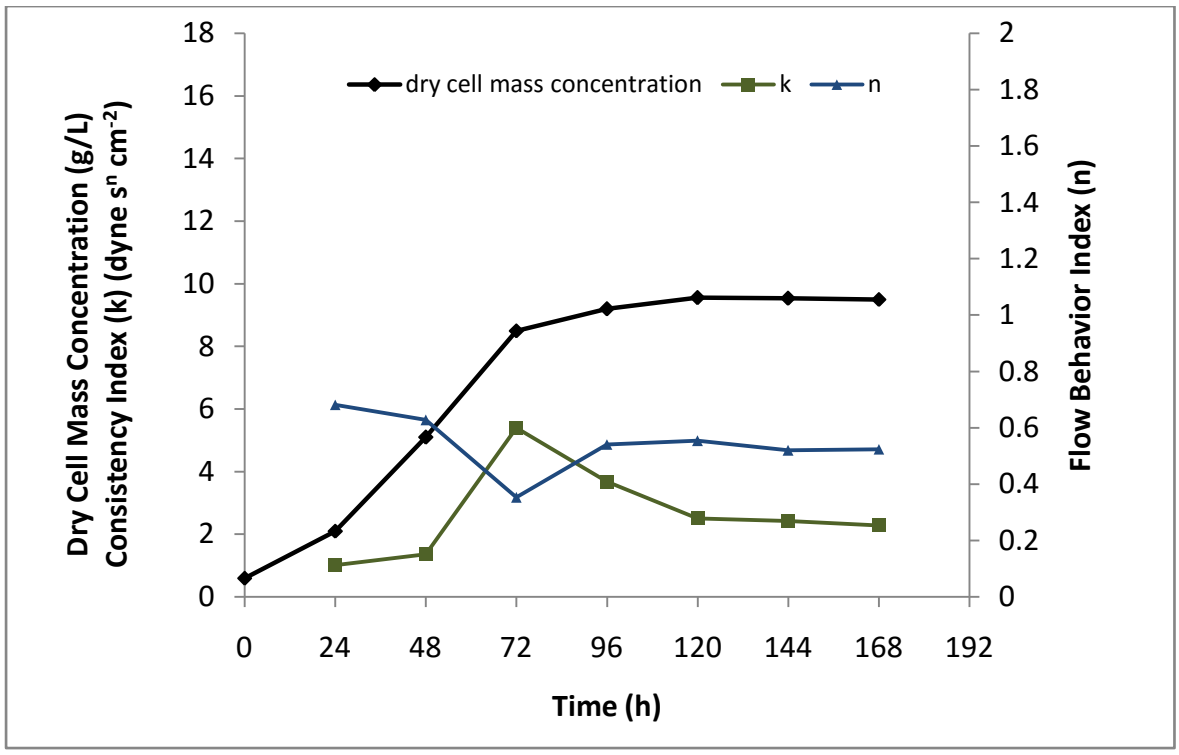

Fig 4.30 Comparison of flow behavior index (n) and consistency index (k) for fed-batch fermentation
Concentration of dry cell mass (filled ◊); consistency index (filled □); flow behavior index (filled Δ)

4.4 Purification of rapamycin

Among all the strategies adopted to evaluate their effect on production of rapamycin, the maximum product concentration was obtained in fed –batch. Therefore, purification of the fermentation broth was carried out using previously established methodology [Patil *et al.*, 2010]. The steps of purification have been summarized in Fig 4.31.

4.4.1 Solvent extraction

Purification was carried out by extraction of the broth using ethyl acetate as solvent by using separating funnel and the extract was then concentrated using vacuum rotary evaporator. The sample was then extracted with acetonitrile three times and then concentrated.

The extract so obtained was then subjected to High Performance Thin Layer Chromatography. HPTLC was carried out to determine the presence of rapamycin in the extract.

Thus, when the peaks of sample and standard were compared, it was found that both have the same value of retention factor (r.f.) as shown in Fig 4.32. One of the bands in sample track of HPTLC plate showed r.f. value 0.20 which was also the r.f. value of the standard peak, which confirmed that rapamycin is present in the extract.

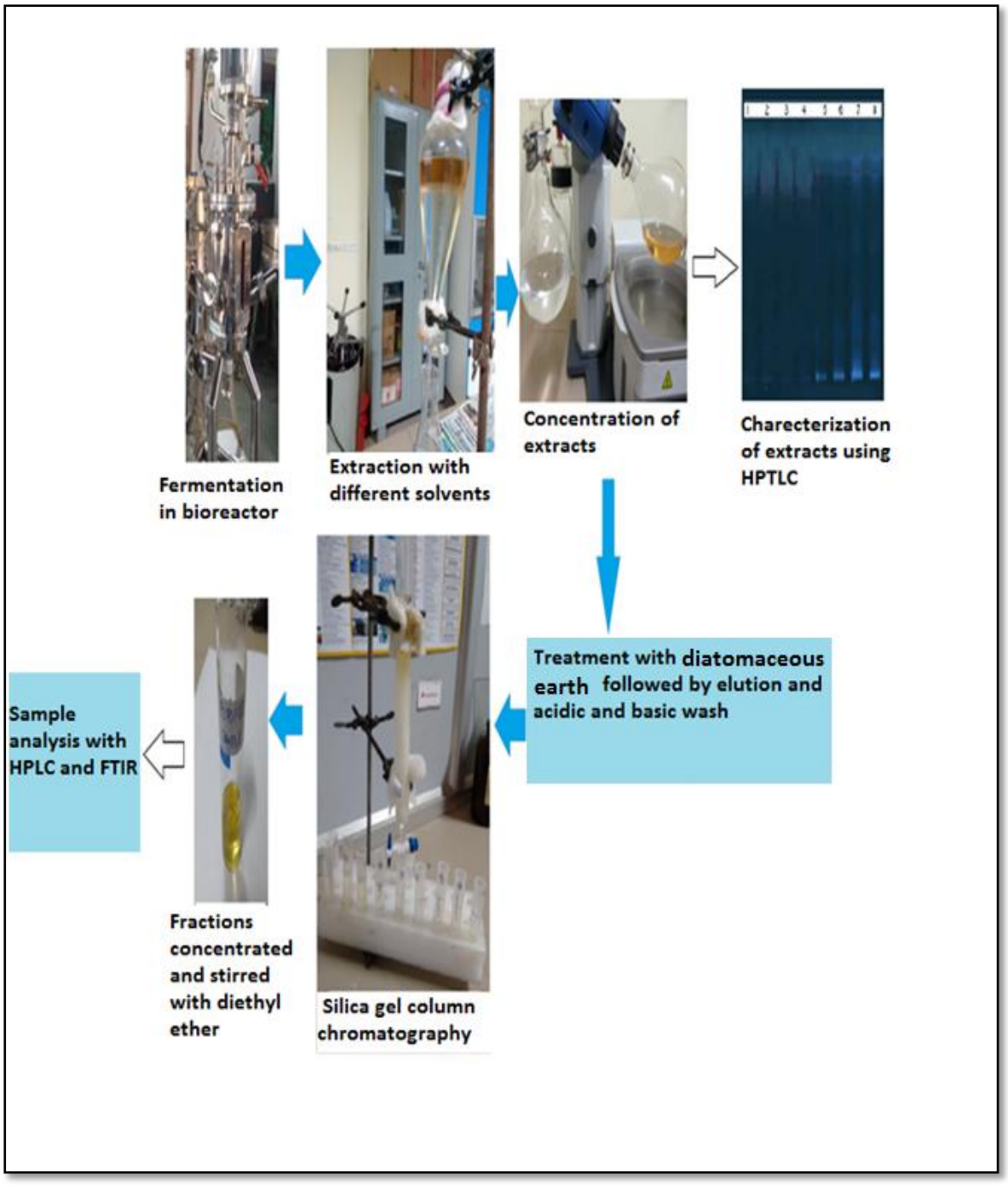

Fig 4.31 Summary of steps followed for rapamycin purification

4.4.2 Purification using silica gel column chromatography

The extract was then purified further by removing the colored impurities with the help of diatomaceous earth and was subjected to acidic and basic wash. The sample was then subjected to acidic and basic wash. Then it was washed several times with distilled water to neutralize the pH of the sample. The sample was then concentrated and subjected to column chromatography. Silica column was prepared and washed with 15% acetone in hexane followed by 25 % acetone in hexane. The product was eluted using 40% acetone in hexane. As the sample was eluted out from the column, different fractions each of 5.0 mL volume were collected. The flow rate during elution was kept as 2.0 mL/min. Each fraction was analyzed for rapamycin content. Fig 4.33 shows the concentration of rapamycin in each fraction. Fractions no. 4 to 15 were found to contain rapamycin.

All the fractions containing rapamycin were pooled together and then concentrated to obtain oily residue. The sample so obtained was stirred in diethyl ether at 4°C to get white coloured suspension of rapamycin which was characterized further.

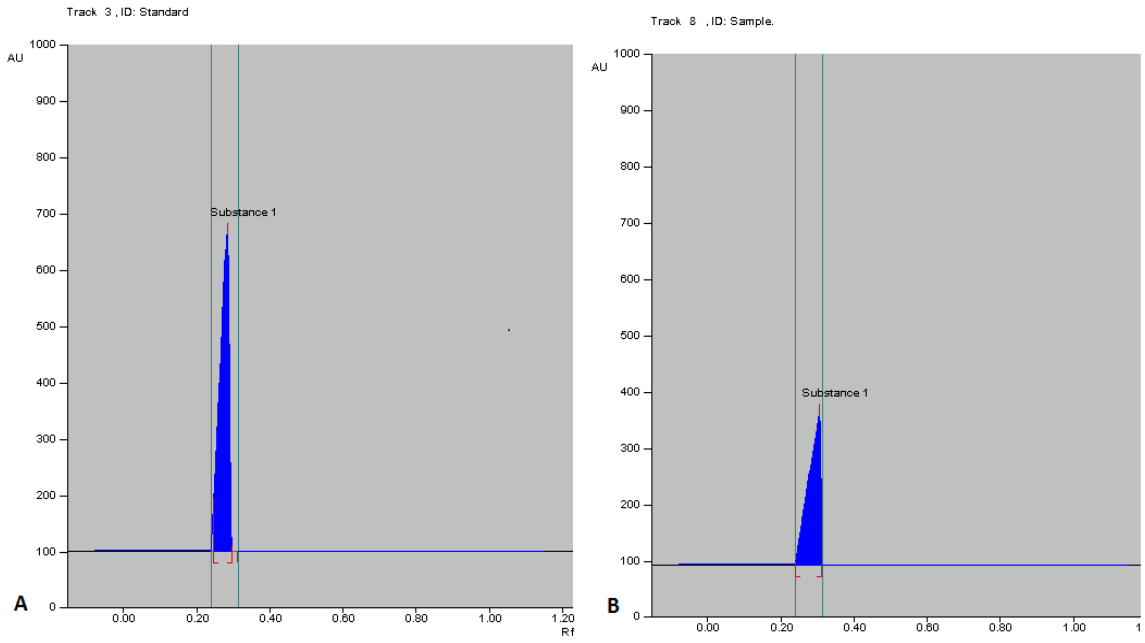

Fig 4.32 HPTLC chromatogram showing A: Peak of Standard at having RF value 0.20 B) Peak of sample at having RF value 0.20

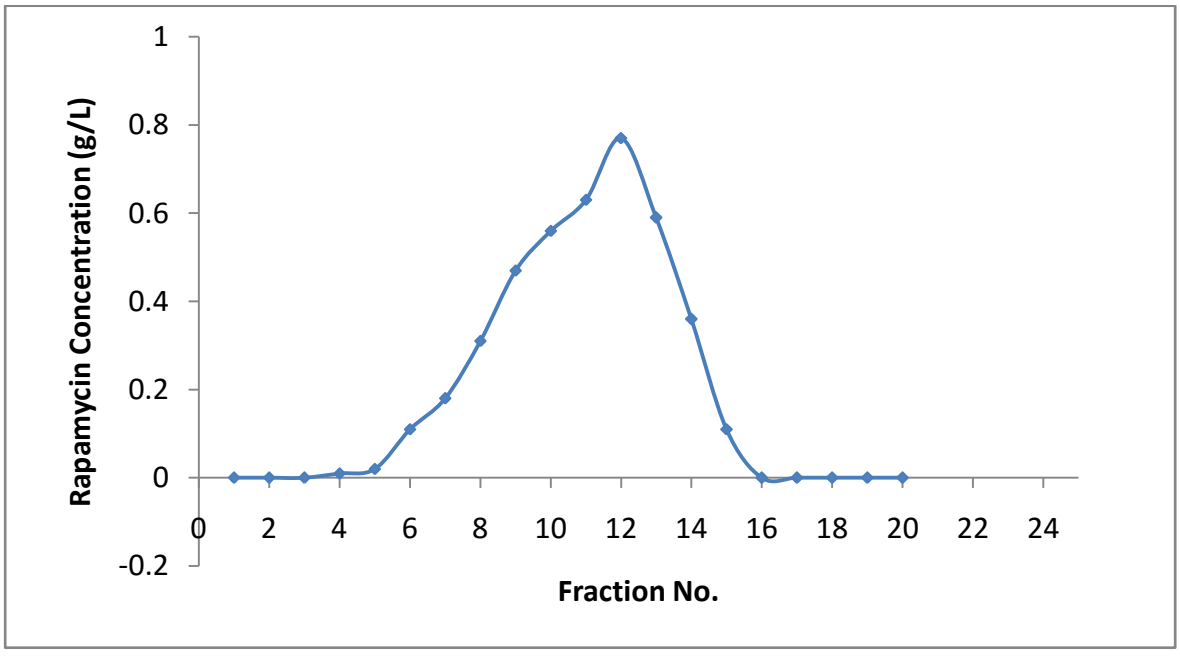

Fig 4.33 Elution profile of rapamycin by silica gel column chromatography

4.4.3 Qualitative characterization of purified sample using FTIR

Purified sample was characterized with the help of Fourier transform infra red (FTIR) spectroscopy (Shimadzu). With the help of FTIR the characteristic functional groups found in rapamycin sample and standard were determined and compared with each other. FTIR spectra both for standard and sample were obtained in which transmittance (%) was plotted against wave number (cm^{-1}) after 45 scans. Fig 4.34 shows the comparison of the FTIR spectra of standard rapamycin and the purified sample. It can be observed that a peak was observed at 1029.07 cm^{-1} which means presence of a -COH stretch. Similarly peak at 1113.94 cm^{-1} represented –COC- stretch. Whereas, two peaks at 1413.88 and 1461.14 cm^{-1} showed presence of -C=C-/ $-CH_3$ bending. Another pair of peaks at 2835.48 and 2948.32 cm^{-1} indicated the presence of –CH stretch. Transmittance peak at 3405.47 cm^{-1}denotes –OH group of the compound. Thus, purified sample was found to contain rapamycin as the FTIR spectrum showed the presence of the characteristic functional groups as well as was found to be significantly similar to the spectrum of the standard compound.

4.4.4 Quantitative analysis of the purified sample using HPLC

Samples obtained after solvent extraction and final purification steps were analyzed quantitatively using HPLC (Waters). Retention time of the samples was compared to the standard rapamycin. Percentage purity of the sample after both stages of purification was calculated. Fig 4.35 shows the chromatogram of samples obtained after solvent extraction and final purification step. Fig 4.35 (A) depicts that standard rapamycin had single peak at retention time 3.195 min. After ethyl acetate extraction, the sample had more than one peak containing rapamycin and other impurities. At this stage sample was found to contain 45% pure rapamycin.

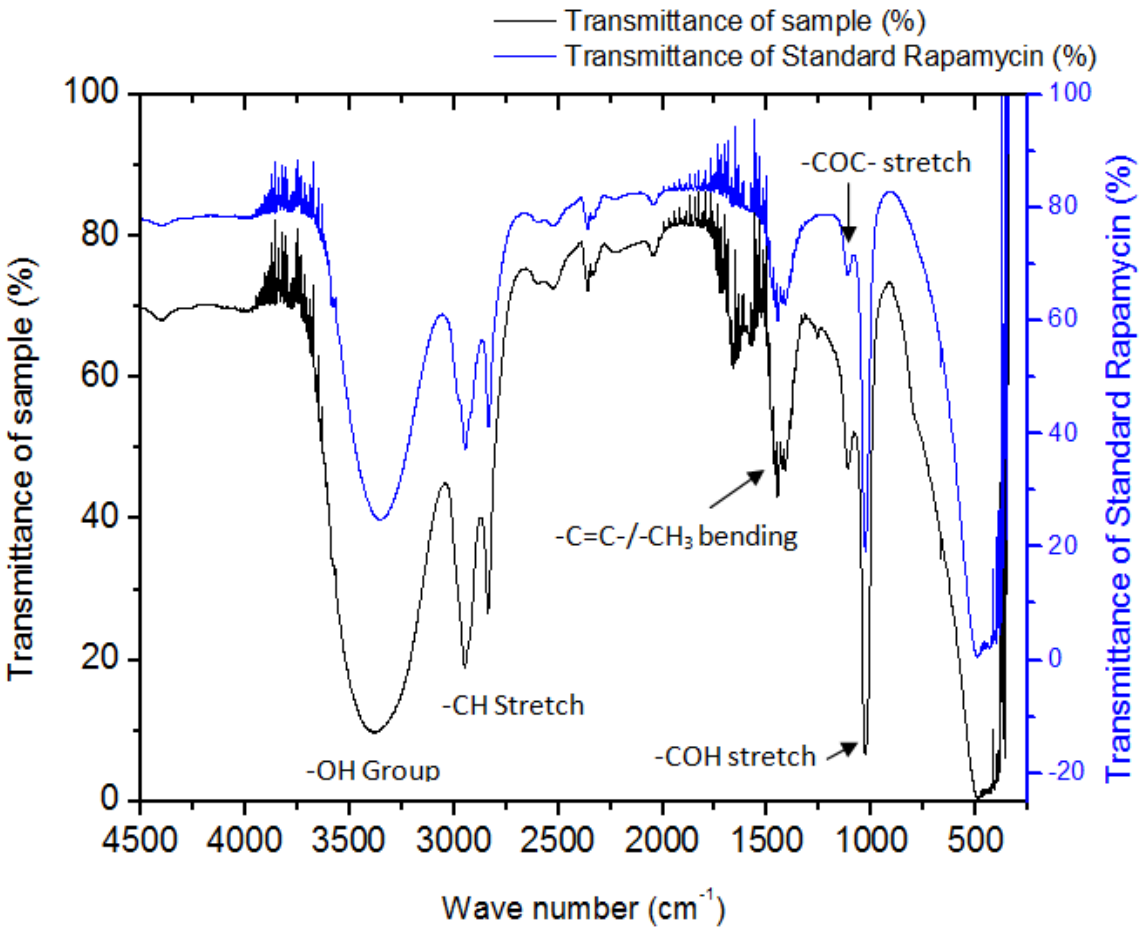

Fig 4.34 Overlay diagram of FTIR spectra of standard rapamycin and the purified sample

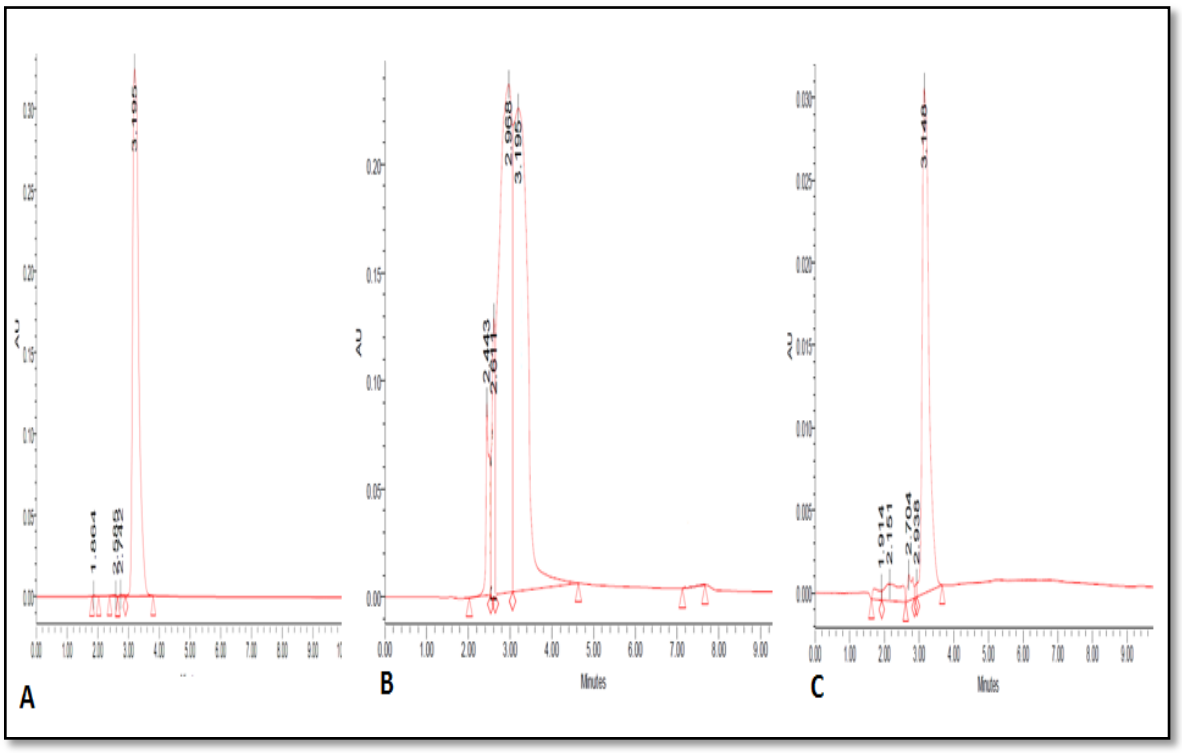

Fig 4.35 HPLC chromatograms (A) Standard rapamycin (B) Ethyl acetate extract (C) Purified sample

Table 4.13 Percentage of rapamycin extracted from broth during purification steps

	Extraction with Ethyl Acetate	Extraction with Acetonitrile	Silica gel Chromatography	Purified sample
Rapamycin extracted (%)	96.7	91.5	85.4	82.3

The results in Fig 4.35 show that after subsequent steps of purification the sample contained 88% of rapamycin and showed peak at similar retention time as that of sample. Each step of purification causes some loss to the original concentration of the product. Table 4.13 shows that after final purification step there was 17.7% loss in the rapamycin concentration.